Elastic and Plastic Structural Response of Tubes to Deflagration-to-Detonation Transition

J. E. Shepherd and F. Pintgen
Graduate Aeronautical Laboratories
California Institute of Technology
Pasadena, CA 91125

Explosion Dynamics Laboratory Report FM2006-005

January 27, 2007

Abstract

The structural response of a tube to an internal loading of a deflagration-to-detonation transition (DDT) event is examined in the plastic and elastic regimes. A single degree of freedom model to used to predict elastic and plastic deformation of the tube. The predicted deformations based on experimental pressure traces are found to be in good agreement with the experimentally-measured deformation. The P-I diagrams give a quick overview of the deformation to be expected for a loading of with a decaying pressure pulse of peak pressure P and impulse I. The scaling of the maximum strain is discussed using models of energy absorption by elastic and plastic deformation. Two-dimensional elastic and plastic finite element simulations are carried out to investigate the effect of the spatial extent of the loading.

Contents

List of Figures

List of Tables

1 Introduction

An important aspect of the analysis of the consequence of explosion hazards is the prediction of the structural response, particularly the possibility of either plastic deformation or rupture of vessels due to internal explosions. The most difficult type of explosion hazard to analyze is deflagration to detonation transition or DDT. The occurs when a low-speed flame accelerates due to a combination of flame instability and turbulence generation and the resulting high speed flame suddenly transitions to detonation.

Previous studies on designing detonation tubes (Shepherd, 1992) have identified plastic deformation and fracture (Chao and Shepherd, 2005b) as important failure modes that can result from DDT. One key issue in explosion analysis is the question of the ability of plastic deformation to accommodate the high pressures produced by DDT without causing catastrophic failure, i.e., rupture. This is important for accidental explosions that would result in the release of hazardous materials. At present, there is no provision within the ASME Boiler and Pressure Vessel or Piping Codes for designing pressure vessels or piping to withstand detonations through plastic response. Currently, a standard is under consideration for designing high-explosive containment vessels based on extensive work by Los Alamos (Duffey et al., 2002, Rodriguez and Duffey, 2004) to formulate ductile failure criteria. Although focused on high explosives, the material response aspect of the Los Alamos work is quite relevant to the present study. The most important aspect of this is the reliance on ideas from modern fracture mechanics (Pellini, 1973) to design vessels that will plastically deform but not catastrophically fail under extreme impulsive loading.

The first section of this report deals with single degree of freedom models for elastic and plastic response of tubes. The second section deals with static response of tubes.

2 Single Degree of Freedom Model

The simplest model of structural response of a tube to explosive loading is to assume a cylindrical shell structure under an axi-symmetric internal load that has a time dependence but a fixed spatial extent. Actual explosion loads vary in both time and space but in order to treat the problem with simple methods, we have ignored the spatial aspects in the present study. In previous studies (Beltman et al., 1999, Beltman and Shepherd, 2002, Chao and Shepherd, 2005a) of elastic response of tubes to shock and detonation waves, the spatial-temporal aspects of the loading were considered in some detail.

The use of simplified models for elastic (Biggs, 1964) and plastic deformation (Jones, 1989) has a long history in mechanics and has been successfully applied to internal explosive loading of cylinders by Duffey and Mitchell (1973) and Benham and Duffey (1974). The goal is to find approximate loading models that will simulate the plastic deformations observed in DDT tests. Detailed considerations of plastic deformation in spherical (Auslender and Combescure, 2000) and cylindrical shells (Nowacki, 1978) reveal that on the time scale of the structural vibrations, stress wave propagation in the radial direction is fast and inertia can be neglected in the computation of radial stress. For example, for a 1.5 mm thick steel tube that is 63.5 mm in radius, the axi-symmetric radial vibrations (Blevins, 1979, Chap. 12) of a long (axially unconfined) cylinder have a fundamental frequency of

$$f = \frac{1}{2\pi R}\sqrt{\frac{E}{\rho(1-\nu^2)}}\ , \tag{1}$$

which results in a frequency of

$$f = 13.7 \text{ kHz} \tag{2}$$

corresponding to an oscillation period of

$$T = 1/f \tag{3}$$

which is numerically equal to

$$= 73.1\ \mu\text{s}\ . \tag{4}$$

The time required for elastic wave transit time through the thickness h is

$$\tau_{wave} = h/c_l \ , \tag{5}$$

where the longitudinal sound speed $c_l = 6100$ m/s for steel, so that

$$\tau_{wave} = 0.25 \ \mu\text{s} \tag{6}$$

or

$$\tau_{wave} \ll T \ . \tag{7}$$

This circumstance greatly simplifies the mathematical treatment of thin cylinders since variation of stress in the radial direction can be either treated quasi-statically (Auslender and Combescure, 2000) or eliminated from consideration entirely by using methods of shell theory (Jones, 1989, Duffey and Mitchell, 1973, Benham and Duffey, 1974)

Assuming radially symmetric and axially uniform loading of an infinite tube structure corresponds to a single degree of freedom (SDOF) model where only radial displacement x of the thin shell structure is permitted, Fig. 1. This loading condition is identical to a circular ring under uniform internal radial pressure. The dynamic behavior of the SDOF model is governed by the balance of force equation in the radial direction (Jones, 1989, Chap. 5) based on the simplest shell theory, neglecting the effects of axial stress, bending or rotary inertia,

$$\rho h \frac{\partial^2 x}{\partial t^2} = -\frac{1}{R} N_\theta + P(t) \ . \tag{8}$$

The density of the tube material is ρ, h is the wall thickness of the tube, R the tube radius and $P(t)$ the time dependent internal pressure loading. The membrane force per unit length (stress resultant) N_θ is usually given in term of the average membrane stress σ as

$$N_\theta = h\sigma \tag{9}$$

so that the force balance can be written

$$\rho h \, \frac{\partial^2 x}{\partial t^2} + \frac{h}{R} \sigma = P(t) \ . \tag{10}$$

In general, the membrane (hoop) stress σ is considered to be a function of the radial strain ϵ, and rate of strain $\dot{\epsilon}$,

$$\sigma = \sigma(\epsilon, \dot{\epsilon}) \ , \tag{11}$$

and in the most general formulations, the thermodynamic state, particularly the temperature.

We will treat the cases of elastic and plastic motions separately. The plastic case is more complex and we defer that until later. For elastic motions, the stress-strain relationship can be substantially simplified although obviously the results are limited in application to small strains ($\epsilon \leq 0.002$) resulting in stress states within the yield surface, roughly speaking $\sigma \leq \sigma_y$, the yield stress. For the simple geometry we are considering, the membrane stress resultant in a cylinder can be written in terms of the hoop strain as (Soedel, 2004, p. 94)

$$N_\theta = K\epsilon_\theta \tag{12}$$

where the membrane stiffness is defined as

$$K = \frac{Eh}{1-\nu^2} \ . \tag{13}$$

The membrane stress is

$$\sigma = \frac{E}{1-\nu^2}\epsilon_\theta \tag{14}$$

where the hoop strain is

$$\epsilon_\theta = \frac{x}{R} \tag{15}$$

and E the modulus of elasticity (Young's modulus). The radial deflection can therefore be modeled as a forced harmonic oscillator,

$$\frac{\partial^2 x}{\partial t^2} + \omega^2 x = \frac{P(t)}{\rho h} \ , \tag{16}$$

where the oscillator natural frequency (radian/s) is

$$\omega = \sqrt{\frac{\bar{k}}{\bar{m}}} \tag{17}$$

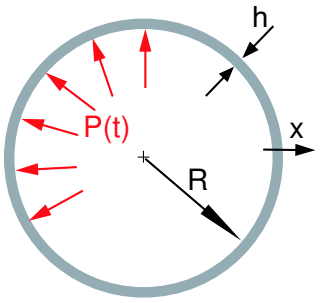

Figure 1: Single degree of freedom model of cylindrical tube structure; radius R, internal pressure $P(t)$, wall thickness h, and radial displacement x.

in terms of the reduced mass $\bar{m} = \rho h$ and the reduced stiffness $\bar{k} = Eh/R^2(1-\nu^2)$. This is related to the usual oscillator frequency f in Hz through

$$\omega = 2\pi f \tag{18}$$

and f is given by Eq. 1.

Table 1 summarizes the dimensions and natural periods for two tubes used for detonation and DDT studies at Caltech.

	R (mom)	h (mom)	R/h	T (μs)	Material
CIT thin	63.5	1.6	38	73	C1010 cold rolled
CIT thick	63.5	12.7	5	73	316 SS

Table 1: Dimensions and periods of tube structures under consideration in this study.

2.1 Elastic regime

The SDOF model for elastic systems is discussed in great detail by Biggs (1964, Chap. 2) for a variety of forcing functions and specifically for high explosives in spherical vessels by Duffey et al. (2002, Part 1.). We only sketch out the essential results here for a single type of forcing function, the rectangular pulse. Results for other pulse shapes, the inclusion of damping, and elasto-plastic models are discussed in depth by Biggs (1964). Applications of SDOF modeling to shock and blast loading are given by Baker et al. (1983).

A program was written using MATLAB and Simulink[1] to numerically solve the equation of motion of the SDOF model, Eq. 16, for arbitrary forcing functions $P(t)$. As an example,

[1]Simulink is a platform for multidomain simulation and Model-Based Design for dynamic systems and is integrated with MATLAB, a high-level language and interactive environment. Both are available from `http://www.mathworks.com`

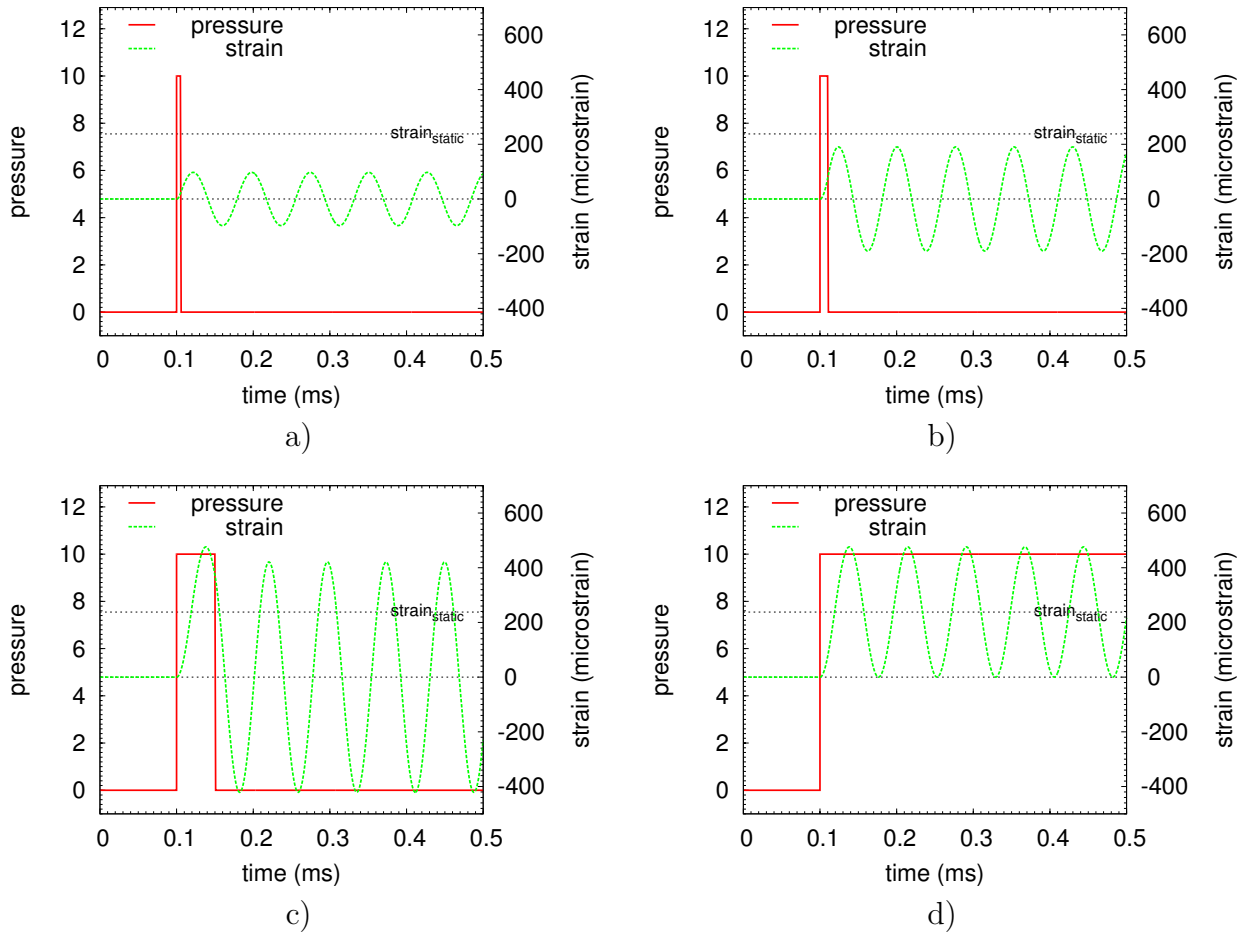

Figure 2: Predicted (SDOF model) response of CIT "thick tube" to a rectangular pressure pulse of 10 MPa and various pulse durations τ a) $\tau = 5$ μs. b) $\tau = 10$ μs. c) $\tau = 50$ μs. d)$\tau = \infty$, step function.

we examined the response of the CIT thick-tube to a rectangular-pulse pressure loading profile with a peak pressure of $P_p = 10$ MPa. The response to pulse durations of 5, 10, 50, and ∞ μs are shown in Fig. 2. In all cases, we see that an oscillatory motion of the tube radius is produced. Of greatest interest for the structural failure analysis is the peak value of the strain. For a fixed peak pressure, the peak strain increases with increasing duration of the pulse. There are two extreme cases, long and short pulses. Long or short is measured by comparing the pulse duration with the shell natural oscillation period, 76 μs for the CIT thick-tube.

2.1.1 Long pulse

When the pulse duration is comparable to or longer than the period of the natural oscillation frequency of the tube, the peak amplitude of the strain appears to be independent of the load

duration. This is sometimes referred to as the sudden or step-loading regime. This should not be confused with the static loading regime, which can be approached either by adding damping to the SDOF model with step loading or slowly ramping the applied pressure up to a constant value.

For infinite pulse duration, Fig. 2d, it can be shown analytically (Biggs, 1964) that the peak hoop strain ϵ_{max} is equal to twice the hoop strain ϵ_{static} for static response with a constant internal pressure equal to the peak loading pressure P_m. The overshoot is due to the inertia of the tube, lack of any damping, and the resulting oscillatory nature of the SDOF solution. The conventional way to characterize the strains in the SDOF model is to define a Dynamic Load Factor (DLF)

$$DLF = \epsilon_{max}/\epsilon_{static} \tag{19}$$

where the static strain for a thin shell is determined from the static solution (see Section 3) to Eq. 10 with a constant pressure $P = P_m$

$$\sigma_{static} = P_m \frac{R}{h} \, , \tag{20}$$

and the corresponding hoop strain is defined by Eq. 14

$$\sigma_{static} = \frac{E}{1-\nu^2}\epsilon_{static} \, , \tag{21}$$

so that the static strain is

$$\epsilon_{static} = \frac{1-\nu^2}{E} P_m \frac{R}{h} \tag{22}$$

and actual peak strain can be expressed as

$$\epsilon_{max} = DLF \frac{1-\nu^2}{E} P_m \frac{R}{h} \, . \tag{23}$$

For a step-load, the maximum strain occurs on the first cycle of oscillation (Biggs, 1964, p. 46) and $DLF = 2$.

2.1.2 General Case

For more complex loads and real structures, interference between modes of vibration can result in the peak strain occurring on a later cycle, a phenomena referred to as strain growth

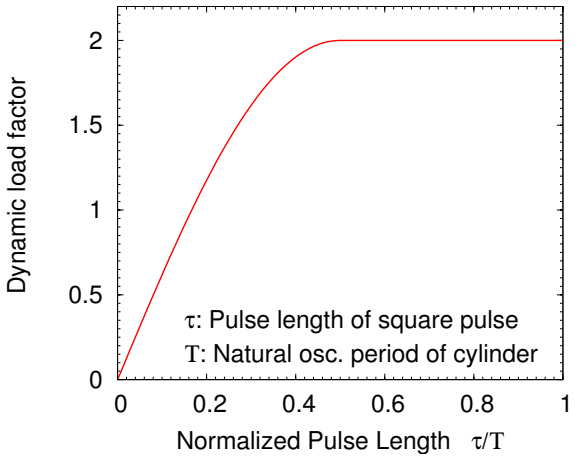

Figure 3: Dynamic Load Factor for a rectangular pulse in elastic regime as function of pulse duration τ.

by Duffey et al. (2002). In general, the DLF will be less than 2 and depends on the details of the forcing function. A wide range of values and dependence on the forcing function parameters is observed for general pulse shapes (Biggs, 1964). For the present case, the DLF can be expressed solely as a function of τ/T (See Appendix A) and is a monotonic function. Computation for a wide range of values of τ/T results in the functional dependence shown in Fig. 3. For long pulses, $\tau > 0.4T$, the $DLF \rightarrow 2$ independent of τ for sufficiently long pulses. For short pulses, $\tau < 0.3T$, the DLF decreases with decreasing pulse duration, this is the impulsive regime, discussed next.

2.1.3 Short pulse

If the rectangular pulse duration is shorter than approximately one-half the natural period of the shell structure, the observed peak strain is smaller than the $2\epsilon_{static}$, Fig. 2a and b, and decreases linearly with decreasing τ. The nearly linear dependence between peak strain and pulse duration τ shown in Fig. 3 can be best explained using the concept of energy conservation from elementary mechanics.

A short pulse will impart an impulse to the shell and set the shell into radial motion. If the duration of the pulse is sufficiently short, then the shell will not move during this time and the effect of the impulse is to set up an initial velocity, corresponding to the transfer of kinetic energy to shell. In the case of elastic motion, the total energy is made up of both kinetic energy and the elastic strain energy of the structure. At the point of maximum deformation, the kinetic energy is converted entirely to strain energy. This concept can be used to determine the relationship between impulse and maximum strain and extended to

also deal with the plastic deformation case.

The mechanical impulse per unit area on the shell is

$$I = \int_0^\infty P(t)\, dt \tag{24}$$

which for a rectangular pulse is just

$$I = P_m \tau \ . \tag{25}$$

From the force balance, this imparts a velocity

$$\mathrm{v}_o = \frac{I}{\bar{m}} \tag{26}$$

to the shell. The kinetic energy $\mathcal{K}$ per unit shell area after absorbing the impulse I is given by

$$\mathcal{K} = \frac{1}{2}\bar{m}\mathrm{v}_o^2$$

or

$$= \frac{I^2}{2\rho h} \ . \tag{27}$$

The strain energy $\mathcal{S}_e$ per unit shell area is

$$\begin{aligned} \mathcal{S}_e &= \frac{1}{2}\bar{k}x_{max}^2 \\ &= \frac{1}{2R^2}\frac{Eh}{1-\nu^2}(\epsilon_{max}R)^2 \end{aligned}$$

or

$$= \frac{1}{2}\frac{Eh}{1-\nu^2}\epsilon_{max}^2, \tag{28}$$

where x_{max} is the maximum displacement, and ϵ_{max} the corresponding maximum strain. For an elastic system, the sum of the strain energy and kinetic energy is the total energy, a constant since energy is conserved. Initially, the energy is all kinetic at the instant just after the impulse is delivered to the system. When the system reaches the maximum deflection, the energy is all strain. This enables the computation of the peak strain by equating the

initial kinetic energy $\mathcal{K}$ and the peak strain energy $\mathcal{S}_e$

$$\frac{I^2}{2\rho h} = \frac{1}{2}\frac{Eh}{1-\nu^2}\epsilon_{max}^2 \ , \tag{29}$$

which shows that the peak strain depends linearly on the impulse in this limit

$$\epsilon_{max} = \sqrt{\frac{1-\nu^2}{Eh^2\rho}} I \ . \tag{30}$$

For rectangular-pulse loading, this is

$$= \sqrt{\frac{1-\nu^2}{Eh^2\rho}} P_m \tau \ , \tag{31}$$

yielding a linear dependence of the maximum strain on the pulse duration τ for a fixed peak pressure P_m, which is what is observed in the impulsive regime of Fig. 3. Using the definition of dynamic load factor, Eq. 19 and the frequency of oscillation, Eq. 1, the dynamic load factor can be expressed analytically as

$$DLF = 2\pi\frac{\tau}{T} \ , \ \tau \leq 0.4T \tag{32}$$

for the rectangular pulse, showing explicitly the dependence on the ratio τ/T in the impulsive regime.

2.2 Plastic regime

If the stress exceeds a critical value, the stress and strain are no longer proportional. For steels used in pressure vessels, this typically occurs when the strains exceed 0.001-0.002 (0.1-0.2%) and the stress is in excess of the *yield stress* σ_y which is on the order of 30-70 ksi (200-480 MPa). Computing structural response in the plastic regime requires considering both the nonlinear characteristics of the stress-strain relationship for $\sigma > \sigma_y$ and the large deformation of the material, particularly the thinning in the direction transverse to the largest principal stress.

Examples of the stress-strain relationships for mild steel, typical of the tubes used in the present experiments, are shown in Fig. 4a. These curves are plotted using engineering stress and strain units typical of tensile test data. For tension in one dimension, the increment in true strain is defined in terms of the fractional increase in length $d\ell$ in the direction of the

applied stress.

$$\begin{aligned} d\epsilon &= \frac{d\ell}{\ell} \\ \epsilon &= \int_{L_o}^{L} \frac{d\ell}{\ell} \\ &= \ln(L/L_o) \ , \end{aligned} \tag{33}$$

and the engineering strain is defined in terms of the fractional extension relative to the original length

$$e = (L - L_o)/L_o \ , \tag{34}$$

and the true strain is

$$\epsilon = \ln(1 + e) \ . \tag{35}$$

The true stress σ is higher than the engineering stress σ_e, which is calculated from the applied force F and the original cross-sectional area A_o,

$$\sigma_e = F/A_o \ . \tag{36}$$

For stresses encountered in the plastic regime, the solid can be treated as incompressible so that the volume of the sample is constant

$$LA = L_o A_o \tag{37}$$

and the true stress

$$\sigma = F/A \tag{38}$$

can be written in terms of the engineering stress and strain as

$$\sigma = \sigma_e(1 + e) \ . \tag{39}$$

Reducing engineering test data such as that shown in Fig. 4a to true stress and true strain requires some care since under large deformations, multi-dimensional "necking" of tensile stress samples will occur, and the material will be in a state of three-dimensional (tri-

axial) stress rather than one-dimensional (uni-axial) stress. For the purposes of numerical simulation, the relationship between true stress and true strain is required. An example of a true stress-true strain curve for a modern pressure vessel steel is shown in Fig. 4b.

The data of Fig. 4 illustrate several significant issues with plastic response under dynamic loading conditions. First, as shown in Fig. 4a, the yield point depends on the rate of strain, conventionally denoted $\dot{\epsilon}$. A pronounced upward shift in the yield point is observed as a function of increasing strain rate. At strain rates of 100-300 s^{-1}, typical of gaseous detonation loading, the yield point can be almost a factor of three higher than under static loading conditions. Second, as the material yields, the stress increases, an effect known as *strain hardening*. The extent of strain hardening depends strongly on the temperature of the material, Fig. 4b, with larger effects being observed at lower temperatures. Third, the nature of the behavior near the yield point depends strongly on the material. In Fig. 4a, the yield point is quite distinct and followed by a plateau of constant stress, which is very typical of mild steels. In Fig. 4b, the yield point is less distinct and strain hardening occurs immediately so that there is a certain amount of arbitrariness in the definition of yield point. Fourth, the combination of strain hardening with the necking that occurs during plastic deformation results in the phenomenon of *plastic instability*. Plastic instability is manifested by the peak in the engineering stress-strain curve of Fig. 4a. Physically, this translates to a maximum load that the material can support prior to catastrophic failure. For strains less than the plastic instability limit, the structure becomes stronger with increasing load, for strains greater than the plastic instability limit, the structure becomes weaker with increasing load. Plastic instability is what determines the ultimate or rupture strength of a ductile pressure vessel, (Harvey, 1974, Section 2.10.3), under static loading conditions. The limiting value will depend on the material and the geometrical configuration of the vessel, see the discussion in Section 3. For simple tension, plastic instability occurs when $\sigma = \sigma_u$, the ultimate or tensile stress. For cylindrical and spherical vessels, instability occurs for $\sigma_\theta \approx \sigma_u$ (see Section 3), the precise value depending on the strain hardening characteristics.

Rigid-plastic model In our analysis of plastic response, we will consider various approximate models of the stress-strain relationship. In the context of dynamic loading, the need to consider plastic response depends on the maximum strain created by the load. Just as in the elastic regime, the maximum strain will depend on the entire time history of the loading with limiting cases of impulsive and step loading. The simplest model for plastic material behavior is the rigid, perfectly plastic, stress-strain relationship, shown graphically in Fig. 5a. In this model, the material is rigid (no deformation) until the stress reaches the

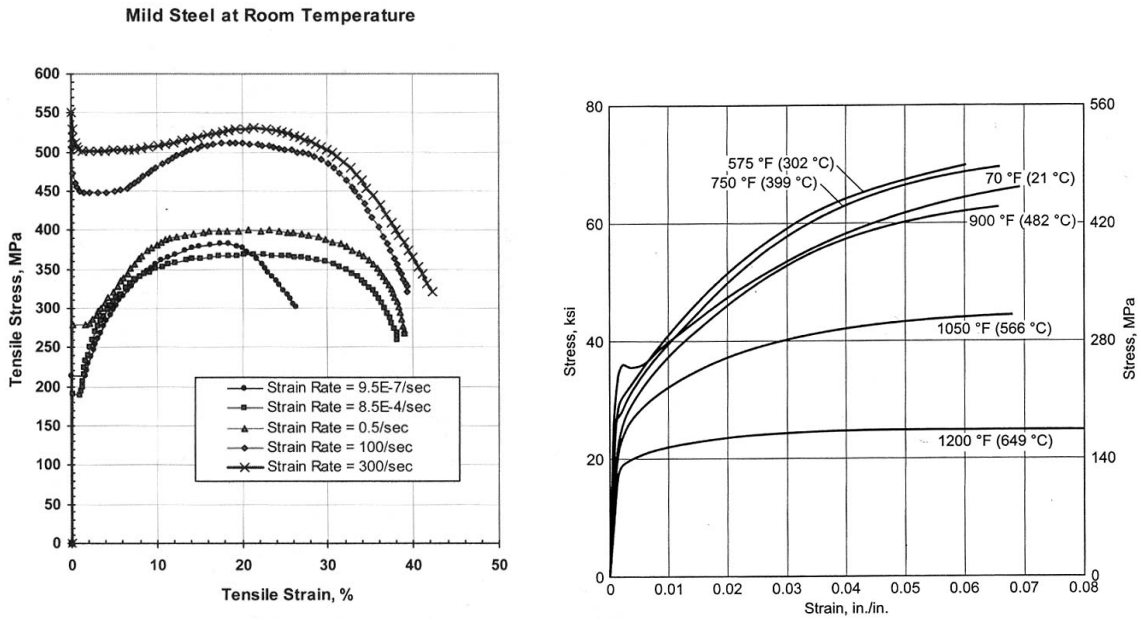

a) b)

Figure 4: Stress-strain relation for a) mild steel (Hampton and Bitner, 2005). b) alloy steel 2.25%Cr 1% Mo (Moosbrugger, 2002).

yield stress

$$\epsilon = 0 \quad \text{for} \quad \sigma < \sigma_y \tag{40}$$

and then the stress is constant and the material permanently deforms with a constant stress for forces that produces stresses in excess of the yield value

$$\sigma = \sigma_y \quad \text{for} \quad \epsilon > 0 \, . \tag{41}$$

If the stress does not exceed σ_y, there is no motion. The rigid-plastic model is useful in obtaining analytical results that give a qualitative guide to behavior. However, more realistic models that include elasticity, strain hardening, and strain rate effects are required for quantitative studies.

Strain-hardening model A more realistic model of plastic deformation needs to include the effects of strain (work) hardening, which are shown in Fig. 4. There are various approximate methods to do this, the simplest being a power law

$$\sigma = K\epsilon^n \, , \tag{42}$$

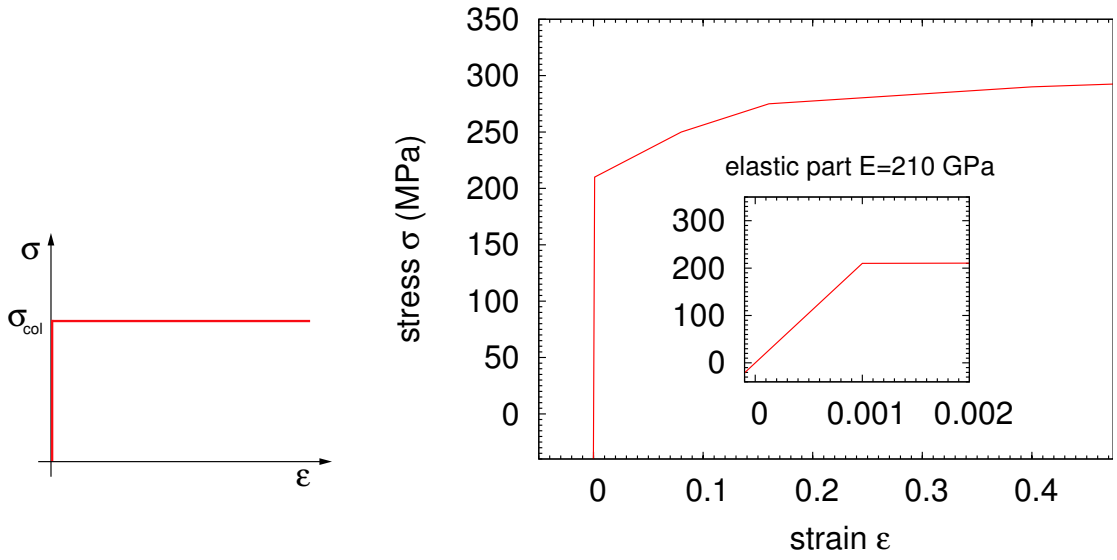

a) b)

Figure 5: Stress-strain relation for a) rigid perfectly plastic material. b) elastic piecewise linear plastic material.

where the exponent n is known as the strain-hardening exponent. This equation and more realistic variations, such as the Swift model

$$\sigma = K(\epsilon_\circ + \epsilon)^n \ , \tag{43}$$

are evaluated against experimental data for stainless steel in Hampton and Bitner (2005), p. 62. For numerical simulations, a common approximation to the stress-strain relationship is the elastic, piecewise-linear plastic, stress-strain relationship, Fig. 5b. As shown, the stress is approximated as a piecewise linear function of strain. The simplest version is to divide the stress-strain curve into two segments, with the material approximated as elastic for small strains

$$\sigma = E\epsilon \quad \text{for} \quad \sigma < \sigma_y \ , \tag{44}$$

and an effective modulus E_1 is used for larger (plastic) strains

$$\sigma = \sigma_y + E_1(\epsilon - \epsilon_y) \quad \text{for} \quad \sigma_y < \sigma \ . \tag{45}$$

In general, more segments can be used for the plastic portion in order to more accurately fit the actual material response. The material used in the CIT thin tube was cold-rolled

steel (C1010), and the yield strength given by the distributer (Marmon Keystone) is σ_y = 210 MPa, and the tensile strength is $\sigma_t = 310$ MPa. In our model, the elastic portion of the response extends from 0< ϵ <0.1%, and the yield point is set to be σ_y=210 MPa. Young's modulus is correspondingly $E = 210$ GPa. If the stress exceeds the yield stress, the material plastically deforms along the piecewise linear curves until the ultimate stress of $\sigma_u = 300$ MPa is reached. Note that the stress-strain relation shown in Fig. 5b represents the true stress-strain relationship or flow-curve. The piecewise-linear plastic stress-strain relationship as shown in Fig. 5b is used in all the numerical simulations carried out in this report.

Strain-rate model To further refine the material model, strain rate effects have to be taken into account. Experimental results (Fig. 4 demonstrate that the stress depends not only on the strain ϵ, but also on the strain rate $\dot{\epsilon}$. The simplest model for accounting for strain rate effects is the Cowper-Symonds model (Cowper and Symonds, 1957), which scales the static yield stress with the factor β,

$$\sigma_y(\dot{\epsilon}) = \sigma_{y,static}\beta \tag{46}$$

where for the present study, the following empirical formula for mild steel is used

$$\beta = 1 + \left(\frac{\dot{\epsilon}}{40}\right)^{0.2} . \tag{47}$$

Strain rate effects have a significant influence on the simulation results for strain rates on the order of $\dot{\epsilon} < 100$ s^{-1}, Fig. 6, since yield strength increases by more than 50% for these conditions. Both the yield stress and ultimate stress increase with increasing strain rate (Hampton and Bitner, 2005, p. 164). Other models for the strain-rate dependence have been proposed and fit to data (Hampton and Bitner, 2005, p. 165-6), notably the Johnson-Cook and Zerilli-Armstrong models.

2.2.1 Static vs. Dynamic Response

For pressure vessels or tubes in the plastic regime, catastrophic failure associated with ductile tearing or plastic instability is usually termed "rupture". For static loading this occurs at the *burst pressure* (Duffey et al., 2002) which depends crucially on the details of the ductility of the material. For dynamic loading, the situation is considerably more complex and depends on the details of the pressure waveform (Florek and Benaroya, 2005) and not just the peak pressure. For high-ductility steels like those used in the present study, substantial deformation and energy absorption can take place in the process of stretching the material

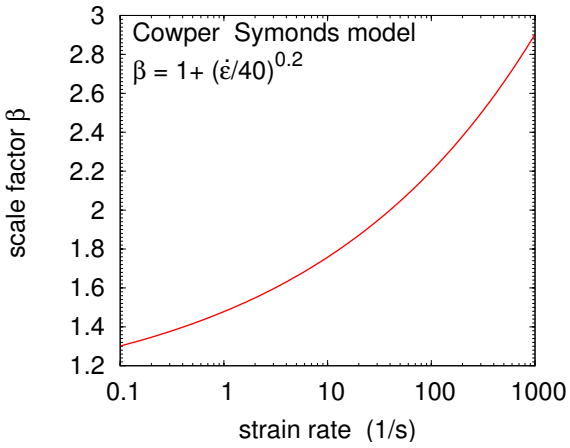

Figure 6: Scale factor β of yield stress σ_y as a function of strain rate $\dot{\epsilon}$, based on the Cowper-Symonds model.

up to the point of rupture.

Duffey et al. (2002) suggest that for dynamic loads it is this ability of a structure to absorb energy through plastic deformation that is most important to designing fracture safe vessels to contain explosive loading. Therefore, they propose that design criteria based on specifying safe levels of plastic strain are most relevant. In the present study, plastic strains of up to 28% are observed without rupture although we are certainly not advocating this as a design limit. An extensive discussion of proposed ductile failure criteria is given by (Duffey et al., 2002).

In a static loading situation, discussed in Section 3, the onset of plastic behavior in the wall of pressure vessel occurs when internal pressure exceeds a critical value, P_y and at a somewhat higher pressure, P_p, the entire vessel wall will be in a state of plastic deformation. If the material exhibits significant strain hardening, then the pressure that results in the onset of the yielding for a structure can be substantially lower than the pressure P_{burst} that results in rupture or burst of the vessel.

In a dynamic loading situation, it is more useful to focus on the peak deformations than the pressures. For elastic analyzes, we introduced the concept of dynamic load factor and used this to estimate peak deformations for a given waveform and peak pressure. For plastic analyzes, the details of the waveform are more important than in the elastic case and it is necessary to consider the motion of the material up to the onset of yielding, the duration of the plastic deformation period, and the subsequent elastic oscillations once plastic deformation has ceased.

Collapse Pressure For thin-tubes, the onset of yielding and fully-plastic state are practically indistinguishable. If strain hardening and elasticity are neglected (rigid plastic model of response) then a single value of internal pressure, the "collapse pressure", can be used to characterize the plastic response. The terminology "collapse" originated in studies of plastic deformation of structures constructed from beams and the formation of mechanisms due to the creation of "plastic hinges" (Jones, 1989). When the applied load exceeds a critical value, the structure is observed to collapse due to the rotation about the hinges. For pressure vessels, a bulge will be created in the wall and in the absence of strain hardening, no quasi-static solution is possible, so the bulge will grow until extensional limit of the material is reached and a rupture is created by a crack extending completely through the wall of the vessel.

In shells, the relationship of the collapse pressure to the membrane forces is not completely straightforward (Jones, 1989, pp. 43-59), but the simplest notion is that collapse begins when the membrane stress reaches the yield strength σ_y of the material. In a static situation, from the time-independent version of the force balance, Eq. 8, we find the often-used approximate relationship for the collapse pressure,

$$P_c = \frac{h}{R}\sigma_y \ . \tag{48}$$

2.2.2 Long Pulse Limit

In the absence of strain hardening, the results can be completely characterized by the the magnitude of the step pressure P_m relative to the collapse pressure P_c corresponding to the onset of yielding.

Elastic, $P_m < 1/2P_c$ For the case of a step load in the elastic regime, we found that the onset of plastic deformation would actually occur for a step pressure P_m that was one-half of the collapse pressure due to the inertia of the shell causing a factor of two overshoot ($DLF = 2$) in the strain.

Elasto-Plastic, $1/2P_c < P_m < P_c$ For a step load in the plastic regime, plastic behavior will commence once the step pressure exceeds one-half of the collapse pressure but only limited plastic deformation will occur as long as the step pressure is less than the collapse pressure. The solution to the ideal elastic-plastic SDOF system is given in Section 2.7 of Biggs (1964). The solution consists of three temporal stages: 1) initial elastic deformation up to the onset of yielding. 2) plastic deformation from the onset of yielding up to the

maximum displacement. 3) elastic oscillations following the achievement of the maximum deflection.

Plastic-rupture, $P_m > P_c$ The plastic deformation continues without bound and the tube ruptures once the extensional limit is reached.

If the material has a significant strain-hardening effect, then the upper limit for elasto-plastic behavior (the rupture limit) will be determined by the rupture or burst pressure of the vessel instead of the onset of yielding.

2.2.3 General Solution

The approximate solution of the SDOF model for a general pulse shape has been considered by a number of authors including Duffey and Mitchell (1973), Benham and Duffey (1974), Hodge (1956), Duffey (1971), Duffey and Krieg (1969), Fanous and Greiman (1988) and others cited in the review by Florek and Benaroya (2005). Under certain assumptions and loading regimes, analytical solutions are possible. We follow the presentation of Benham and Duffey (1974), who neglect the axial stress resultant and bending moment, consistent with a purely radial motion. The equation of motion is the same as Eq. 10

$$\rho h \frac{\partial^2 x}{\partial t^2} + \frac{h}{R}\sigma = P(t) \; .$$

In order to solve this model, a stress-strain $\sigma(\epsilon)$ relationship is required. In general, this requires considering the time history of the deformation if plastic deformation can occur. The plastic deformation is irreversible and changes only when the stress state has reached the yield condition while the elastic component is reversible. The specification of the yield surface and computation of the plastic strain evolution is discussed in Chap. 5 of Johnson and Mellor (1983) and the application to explosively loaded cylinders is given by Duffey and Krieg (1969).

For the cases considered in this study, the loading is quite simple and plastic deformation usually only occurs for a limited duration during the primary pressure pulse associated with the detonation wave. There is an initial elastic phase that initiates the yielding, followed by plastic flow until deformation stops, and then elastic unloading. Strain rate effects are primarily confined to the initial transient and the strain rate has a single characteristic value determined by the resonant frequency of the tube and maximum strain, $\dot{\epsilon} \approx \epsilon_{max}/T$. With these considerations, a simple empirical rule for the flow stress can be used during the

yielding phase of the motion ($\epsilon > \epsilon_y$ and $\dot{\epsilon} > 0$)

$$\sigma = \sigma_y^D \left(1 + \lambda\epsilon\right) \ , \tag{49}$$

and the dynamic yield stress value σ^D which depends on the strain rate. A simple approximation for this is the Cowper-Symonds model mentioned earlier (Eq. 47)

$$\sigma_y^D = \sigma_y \left[1 + \left(\frac{\dot{\epsilon}}{D}\right)^{1/p}\right] \ . \tag{50}$$

where the values of the parameters D and p are determined by fitting experimental data.

Hodge (1956) considers the solution for the case of rigid-plastic model with an arbitrary pressure loading history $P(t)$ and although he was able to make progress, he was unable to find analytical solutions for loads of practical importance. By introducing other approximations, Benham and Duffey (1974) were able to solve the problem analytically by assuming a rigid-plastic linear-hardening model and that the dynamic yield stress was a constant. Including the strain rate dependence of the yield stress required a numerical solution. The inclusion of elastic loading and unloading is discussed by Duffey and Krieg (1969), Duffey (1971). An approximate solution for the final shape of impulsively-loaded long cylinders was obtained by Duffey and Mitchell (1973) for rigid-plastic model with strain hardening and rate effects. Approximate solutions for the maximum deformation of several types of shells under impulsive loading were obtained by Fanous and Greiman (1988). For the present study, instead of carrying out numerical solutions of Eq. 10 directly, we have used a commercial finite-element simulation program to obtain solutions for specific pressure histories of interest and an empirical flow rule for the materials of interest. The results are given subsequently in Section **??**.

2.2.4 Short Pulse Limit

In the impulsive regime, the peak pressure can be comparable to or higher than the collapse pressure and the response can still be in the elastic regime if the impulse is sufficiently low. The purely elastic case was covered in Section 2.1 and some of the same considerations apply here. The impulse I results in an initial velocity $\mathrm{v}_\circ = I/\rho h$ and the subsequent motion of the shell is governed by the unforced equation of motion

$$\rho h \, \frac{\partial^2 x}{\partial t^2} + \frac{h}{R}\sigma = 0 \ .$$

This can be integrated from the initial time up to the maximum displacement to obtain

$$\frac{1}{2}\rho \mathrm{v}_\circ^2 = \int_0^{\epsilon_{max}} \sigma \, d\epsilon \, , \tag{51}$$

which we can interpret as the conversion of the initial kinetic energy (left-hand side) into strain energy (right-hand side). The amount of energy that can be absorbed by elastic motion is limited by the onset of yield at $\epsilon = \epsilon_y$

$$\int_0^{\epsilon_y} \sigma \, d\epsilon = \frac{\sigma_y \epsilon_y}{2} \, . \tag{52}$$

For higher strains, the additional energy is absorbed by elastic deformation until the cylinder wall comes to rest. The total amount of plastic work is

$$\int_{\epsilon_y}^{\epsilon_{max}} \sigma \, d\epsilon \, . \tag{53}$$

If the maximum deformation is significantly larger than the yield value, then the energy absorbed by the elastic motion can be neglected in comparison to the plastic deformation. With this approximation, the peak deformation can be estimated from the conservation of energy using the rigid plastic material model

$$\begin{aligned} \frac{1}{2}\rho \mathrm{v}_\circ^2 &\approx \int_0^{\epsilon_{max}} \sigma_y \, d\epsilon \\ &= \sigma_y \epsilon_{max} \, . \end{aligned} \tag{54}$$

solving for the maximum displacement,

$$\begin{aligned} \epsilon_{max} &= \frac{\rho}{2\sigma_y} \left(\frac{I}{\rho h} \right)^2 \\ \epsilon_{max} &= \frac{P_m^2 \, \tau^2}{2\sigma_y \rho h^2} \, . \end{aligned} \tag{55}$$

Based on this simplified material behavior, the maximum strain scales with the square of the impulse I rather than linearly as found in the plastic regime. For a material with strain-hardening and an elastic regime, the maximum displacement can be determined from integration of Eq. 51 and solving the resulting relationship between impulse and maximum strain.

3 Static Cylindrical Tube Response

The static elastic and plastic response of a cylindrical tube is given in in standard textbooks on elasticity, Timoshenko and Goodier (1970), pressure vessel design, Harvey (1974), strength of materials, Ugural and Fenster (1987), and plasticity, Johnson and Mellor (1983). We summarize the formulation and key results here.

3.1 Elastic Response

The elastic response of a cylinder under pressure starts by considering the stress-strain relationships for an elastic solid, the generalized *Hooke's law*, in a cylindrical coordinate system (r, θ, z) - see Fig. 7.

$$\epsilon_r = \frac{1}{E}[\sigma_r - \nu(\sigma_\theta + \sigma_z)] \tag{56}$$

$$\epsilon_\theta = \frac{1}{E}[\sigma_\theta - \nu(\sigma_r + \sigma_z)] \tag{57}$$

$$\epsilon_z = \frac{1}{E}[\sigma_z - \nu(\sigma_\theta + \sigma_r)] \tag{58}$$

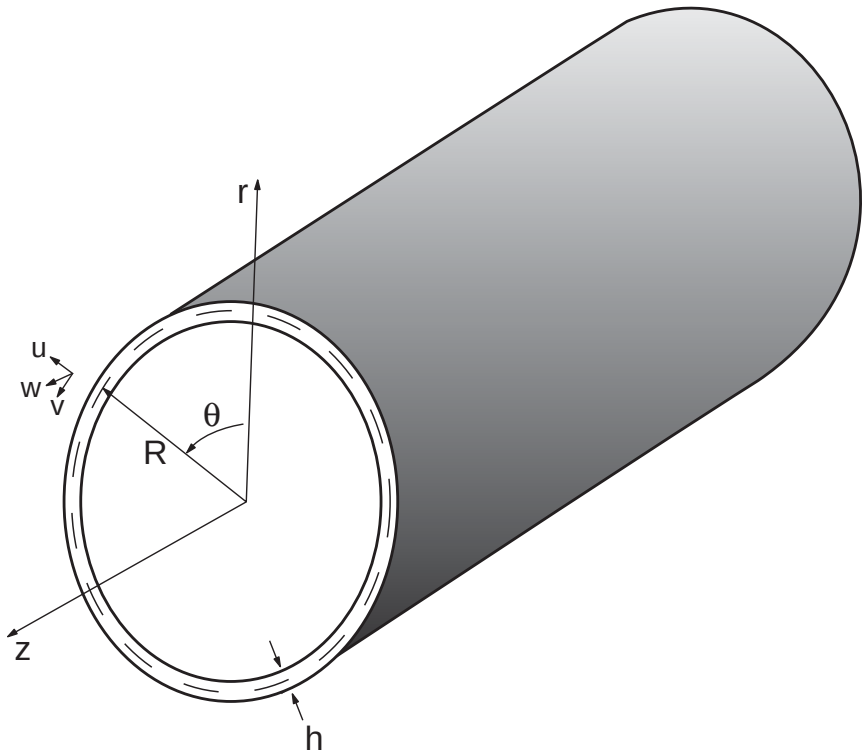

Figure 7: Coordinate system for analysis of cylinder response to internal pressure loading.

For a cylinder, there are two special solutions for the case of a uniform internal and external pressure loads:

1. Plane stress, $\sigma_z = 0$. This corresponds to the ends of the cylinder being free to move so that no stress exists in the longitudinal direction. Physically, this corresponds to the case of a ring with no axial confinement so that the axial stress is zero at the boundaries and either exactly (pure 2-d flow) or approximately zero in the interior.

   For plane stress, the strain-stress relations are:

$$\epsilon_r = \frac{1}{E}(\sigma_r - \nu\sigma_\theta) \ , \tag{59}$$

$$\epsilon_\theta = \frac{1}{E}(\sigma_\theta - \nu\sigma_r) \ , \tag{60}$$

$$\epsilon_z = -\frac{\nu}{E}(\sigma_\theta + \sigma_r) \ . \tag{61}$$

   Note that the stresses (σ_r, σ_θ) completely determine the solution for all strains. Solving for the stresses in terms of the strains, we have

$$\sigma_r = \frac{E}{1-\nu^2}(\epsilon_r + \nu\epsilon_\theta) \ , \tag{62}$$

$$\sigma_\theta = \frac{E}{1-\nu^2}(\epsilon_\theta + \nu\epsilon_r) \ . \tag{63}$$

2. Plane strain, $\epsilon_z = 0$. The corresponds to the ends of the cylinder being fixed so that no axial displacement occurs. Physically, this corresponds to the case of a long cylinder or perfect axial confinement of a ring so that the displacement is zero at the boundaries and either exactly (pure 2-d flow) or approximately zero in the interior.

$$\sigma_z = \nu(\sigma_\theta + \sigma_r) \ , \tag{64}$$

$$\epsilon_r = \frac{(1+\nu)}{E}[(1-\nu)\sigma_r - \nu\sigma_\theta] \ , \tag{65}$$

$$\epsilon_\theta = \frac{(1+\nu)}{E}[(1-\nu)\sigma_\theta - \nu\sigma_r] \ . \tag{66}$$

   Note that the stresses (σ_r, σ_θ) completely determine the solution and the stress σ_z is a consequence of the strains in the other directions. Solving for the stresses in terms

of the strains, we have

$$\sigma_r = \frac{E}{(1+\nu)(1-2\nu)}[(1+\nu)\epsilon_r + \nu\epsilon_\theta] \,, \tag{67}$$

$$\sigma_\theta = \frac{E}{(1+\nu)(1-2\nu)}[(1+\nu)\epsilon_\theta + \nu\epsilon_r] \,. \tag{68}$$

Even with these restrictions on the z-direction, it is also possible for there to be shear $\gamma_{r\theta}$ and a shear stress $\tau_{r\theta}$ in the in the r-θ plane; these are related by

$$\gamma_{r\theta} = \frac{\tau_{r\theta}}{G} \tag{69}$$

where G is the shear modulus

$$G = \frac{E}{2(1+\nu)} \,. \tag{70}$$

The material displacements are (u, v, w) and from the definition of strain, the strains are given by

$$\epsilon_r = \frac{\partial u}{\partial r} \,, \tag{71}$$

$$\epsilon_u = \frac{u}{r} + \frac{1}{r}\frac{v}{\theta} \,, \tag{72}$$

$$\gamma_{r\theta} = \frac{\partial v}{\partial r} + \frac{1}{r}\frac{\partial u}{\partial \theta} - \frac{v}{r} \,. \tag{73}$$

If we suppose that the displacement is only in the r direction (corresponding to symmetry in the circumferential direction), then v =0, $\partial/\partial\theta = 0$, and $\gamma_{r\theta} = 0$, and the equation of force equilibrium in the radial direction is

$$\frac{\partial \sigma_r}{\partial r} + \frac{\sigma_r - \sigma_\theta}{r} + F_r = 0 \,. \tag{74}$$

For static problems in which no external body forces (e.g., the weight of the vessel) are considered, $F_r = 0$. The radial displacement $u(r)$ can be determined by substituting into Eq. 74 the expressions (Eq. 68 or 63) for the stresses in terms of the strains (expressed in terms of the displacements, Eq. 73). The boundary conditions on the radial stresses are given by the applied pressures to the interior ($r = a$)

$$\sigma_r(r = a) = -P_i \tag{75}$$

and exterior ($r = b$) of the cylinder

$$\sigma_r(r = a) = -P_o \ . \tag{76}$$

The cases of plane strain and plane stress will be considered separately. These solutions are known as the Lamé solutions to the elastic thick cylinder problem.

3.1.1 Plane Strain

The stresses are

$$\sigma_r = \frac{E}{1-\nu^2}\left(\frac{du}{dr} + \nu\frac{u}{r}\right) \tag{77}$$

and

$$\sigma_\theta = \frac{E}{1-\nu^2}\left(\frac{u}{r} + \nu\frac{du}{dr}\right) \ . \tag{78}$$

Substituting in the force equation, we have

$$0 = \frac{d^2u}{dr^2} + \frac{1}{r}\frac{du}{dr} - \frac{u}{r^2} \tag{79}$$

which has as solutions

$$u = c_1 r + \frac{c_2}{r} \tag{80}$$

where c_1 and c_2 are constants to be determined by applying the boundary conditions on the radial stress. Doing this, we find the stresses to be

$$\sigma_r = \frac{a^2P_i - b^2P_o}{b^2 - a^2} - \frac{(P_i - P_o)a^2b^2}{(b^2 - a^2)r^2} \ , \tag{81}$$

and

$$\sigma_\theta = \frac{a^2P_i - b^2P_o}{b^2 - a^2} + \frac{(P_i - P_o)a^2b^2}{(b^2 - a^2)r^2} \ , \tag{82}$$

and the radial displacement is

$$u = \frac{1-\nu}{E}\frac{(a^2P_i - b^2P_o)r}{b^2-a^2} + \frac{1+\nu}{E}\frac{(P_i-P_o)a^2b^2}{(b^2-a^2)r} \ . \tag{83}$$

The strain in the z-direction is independent of the coordinate r and is equal to

$$\epsilon_z = -\frac{2\nu}{E}\left(\frac{a^2P_i - b^2P_o}{b^2-a^2}\right) \ . \tag{84}$$

Since the shear stress $\tau_{r\theta} = 0$, the principal stresses are σ_θ and σ_r and the maximum shear stress is

$$\tau_{max} = \frac{1}{2}(\sigma_\theta - \sigma_r) \tag{85}$$

or

$$= \frac{(P_i-P_o)a^2b^2}{(b^2-a^2)r^2} \ . \tag{86}$$

The maximum value of the shear stress occurs at the inner surface.

Thin tube approximation The results can be considerably simplified for large internal pressures $P_i \gg P_o$ and thin-walled tubes b - $a = h \ll R = (b+a)/2$. The radial stress is always on the order of the applied pressure difference

$$\sigma_r \sim \Delta P \ . \tag{87}$$

Applying order-of-magnitude analysis to the radial force equilibrium equation, we find that the tangential stress must be of the order

$$\sigma_\theta \sim \frac{R}{h}\Delta P \ . \tag{88}$$

Algebraic manipulation of the exact solution verifies these order of magnitude estimates and the tangential stress is approximately equal the value given by the membrane theory

$$\sigma_\theta \approx \frac{R}{h}\Delta P \tag{89}$$

and the maximum shear stress is

$$\tau_{max} \approx \frac{R}{2h}\Delta P \ . \tag{90}$$

This approximation improves with increasing values of R/h.

3.1.2 Plane Stress

The relationships for plane stress can either be derived as in the plane strain case or else transformed from the plane strain results using the transformation given in most texts on elasticity, see Table 3.1 on p 71 of Ugural and Fenster (1987). For a thin tube, the key difference is the presence of a stress in the z direction,

$$\sigma_z \approx \frac{R}{2h}\Delta P \ . \tag{91}$$

3.2 Plastic Deformation

The onset of plastic deformation first occurs at the inner most portion of the cylinder. The exact pressure at which yielding first takes place depends on the criteria used to define the yield surface (Ugural and Fenster, 1987, p. 268). A simple condition is that yielding takes place when the maximum shear stress exceeds the shear strength $\tau_y = \sigma_y/2$ of the material. For a thick cylinder under internal pressure only, the innermost "fibers" will yield when

$$\tau_y = \frac{b^2}{b^2 - a^2}P_i \ , \tag{92}$$

and in the thin cylinder approximation, yielding will first occur when

$$\Delta P_y = \frac{h}{R}2\tau_y \tag{93}$$

$$= \frac{h}{R}\sigma_y \ . \tag{94}$$

For a tube with internal pressure only, the yielding will start at the inner surface and with increasing pressure, spread to the outer surface. The radial stress distribution can be obtained for the fully plastic cylinder by approximating the yield condition. Recognizing that the maximum shear stress is

$$\tau_{max} = \frac{1}{2}(\sigma_\theta - \sigma_r) \ , \tag{95}$$

we can rewrite the radial force equilibrium as

$$\frac{d\sigma_r}{dr} = \frac{2\tau_{max}}{r} \ . \tag{96}$$

If we approximate the yield surface with the Tresca condition, $\tau_{max} = \tau_y$, and neglect strain hardening, $\tau_y =$ constant, we can integrate this to obtain

$$\sigma_r = 2\tau_y \ln(r/b) \ , \tag{97}$$

where we have used the approximate conditions that $\sigma_r \sim 0$ at $r = b$. Then, the pressure for which the cylinder is fully plastic is

$$P_p = 2\tau_y \ln \frac{b}{a} \ . \tag{98}$$

For a thin tube, expansion of the logarithm yields

$$P_p \approx 2\tau_y \left[\frac{h}{R} + \frac{1}{3} \left(\frac{2h}{R} \right)^3 + \ldots \right] \ . \tag{99}$$

This implies that for a thin tube, the yielding spreads very quickly through the tube wall and there is little difference between the pressure needed for the onset of yielding and the fully plastic state. Once the tube has fully yielded, if the material is approximated as a perfectly plastic material it will continue to deform as long $P_i > P_p$. There is no static solution in this case since the tube will enlarge until it ruptures once the maximum elongation of the material is reached. A slightly smaller value of critical pressure for fully plastic deformation will be found if the von Mises yield surface is used.

On the other hand, if the material exhibits appreciable strain hardening, then the deformation will reach a static equilibrium as long as the internal pressure is less than some maximum value. If the failure mode is purely ductile, then maximum pressure that the tube can statically withstand will be determined by the onset of plastic instability, which requires considering the details of the actual strain hardening curve. However, it is possible to make a simple estimate of the static *burst pressure* by assuming that at burst, the shearing stresses are uniform over the thickness and equal to the ultimate shearing strength τ_u and that the dimensions of the deformed tube are not too drastically different from the original

$$P_{burst} = 2\tau_u \ln \frac{b}{a} \ , \tag{100}$$

which for a thin tube is

$$P_{burst} \approx \sigma_u \frac{h}{R} \; . \tag{101}$$

If the strain hardening curve can be approximated with a simple power law form, then it is possible to improve on this estimate of bursting pressure by accounting for the change in the thickness of the tube during plastic deformation and for the actual stress distribution. A solution using Hencky's stress-strain relationships is given on p. 396 of Ugural and Fenster (1987); a solution using Lévy-Mises incremental strain relationships is given on p. 402 of Ugural and Fenster (1987) and Chap. 10 of Johnson and Mellor (1983).

For example, using the Lévy-Mises formulation and Swift's form of the strain hardening rule

$$\sigma = K(\epsilon_\circ + \epsilon)^n \; , \tag{102}$$

Johnson and Mellor (p. 264) show that the ordinary or ultimate tensile strength (determined by plastic instability in simple tension) is

$$\sigma_u = K n^n \exp(\epsilon_\circ - n) \; , \tag{103}$$

while the hoop stress for a thin-walled pipe (internal pressure with closed ends, case of plane stress) at instability is

$$\sigma_\theta = P\frac{R}{h} \tag{104}$$

$$= K\frac{2}{\sqrt{3}}\left(\frac{n}{\sqrt{3}}\right)^n \; . \tag{105}$$

The straining of the cylinder increases the radial dimension

$$R = R_\circ \exp(\epsilon_\theta) \tag{106}$$

and makes the wall thinner

$$h = h_\circ \exp(-\epsilon_\theta) \; , \tag{107}$$

where the hoop strain at instability is equal to

$$\epsilon_\theta = \frac{\sqrt{3}}{2}\left(\frac{n}{\sqrt{3}} - \epsilon_\circ\right) \ . \tag{108}$$

The internal pressure at the point of plastic instability is therefore

$$P = \frac{h_\circ}{R_\circ} K \frac{2}{\sqrt{3}}\left(\frac{n}{\sqrt{3}}\right)^n \exp(\sqrt{3}\epsilon_\circ - n) \ , \tag{109}$$

which can be written in terms of the ordinary tensile strength as

$$P = \frac{h_\circ}{R_\circ}\sigma_u \psi \tag{110}$$

where ψ is

$$\psi = \frac{2}{(\sqrt{3})^{n+1}} \exp \epsilon_\circ(\sqrt{3} - 1) \ . \tag{111}$$

The factor ψ is a function of the strain hardening parameters $\epsilon_\circ$ and n. For small values of n, $\psi > 1$ and for large values, $\psi < 1$. For a given n, the value of ψ increases for increasing $\epsilon_\circ$. For typical values of the parameters, ψ can be as much as 15% higher or lower than unity. This shows that basing the burst pressure on the tensile strength (the simplest estimate) can either under- or over-estimate the burst pressure. For example, in 304 SS, the parameters are $n = 0.561$, $\epsilon_\circ = 0.07$, and $K = 1.55$ GPa; in this case $\psi = 0.89$ and $\sigma_u = 685$ MPa.

An empirical formula for the bursting pressure of cylindrical vessels is (Harvey, 1974)

$$P_{burst} = \left[\left(\frac{0.25}{n + 0.227}\right)\left(\frac{e}{n}\right)^n\right]\sigma_u \ln\frac{b}{a} \ , \tag{112}$$

which for thin tubes, reduces to the expression given above with ψ equal to the term in the square brackets. The effective strain hardening exponent n is linearly correlated to the ratio of σ_y/σ_u (Harvey, 1974, Fig. 2.26) and the numerical values of ψ have similar trends with n as in the model results of Johnson and Mellor (1983).

4 Peak Pressure-Impulse Damage curves

In general, in order to estimate the extent of plastic deformation from a specific pressure history, it is necessary to carry out numerical simulations for that case. In a hazard analysis, it is desirable to examine the consequences of a range of pressure waveforms that bound the possible outcomes of postulated accident events. For this purpose, a more rapid means of analysis is desirable in order to make bounding estimates. One technique that is widely used (Baker et al., 1983, Florek and Benaroya, 2005) in blast wave loading and structural damage prediction is to characterize the pressure waveform with the peak pressure P and impulse I. A pressure waveform shape is assumed, parameterized with P and I, and computations are carried out to obtain contours of constant damage or iso-damage (deformation in the present case) as a function of these two parameters.

These iso-damage maps are known as P-I diagrams and are widely used in hazard analysis to evaluate the potential for damage to structures and people from blast loading. For large values of P or I, the results appear to relatively independent of the waveform shape (Baker et al., 1983, Florek and Benaroya, 2005) which makes this technique very appealing for quick evaluation of hazards. The results are also in reasonable agreement with experimental data and simple structural models that show damage can be correlated with exceeding critical values of either peak pressure (long pulse limit) or impulse (short pulse limit). However, for intermediate values of P and I, the results are strongly waveform shape dependent, particularly for plastic deformation (Florek and Benaroya, 2005). The reason for the extreme sensitivity of the deformation to loading in the plastic regime is due to the shallow slope of the strain hardening curve, Fig. 5, leading to large differences in final deformation for modest changes in peak pressure. Another way to conceptualize this is that the effective modulus for plastic deformation is much smaller than for elastic deformation.

Based on the appearance of the experimental data, we have assumed a pressure pulse that consists of a jump followed by an exponential decay

$$P(t) = P_{max} \exp\left(-t/\tau\right), \tag{113}$$

where τ is the characteristic decay time of the pressure signal and P_{max} is the peak pressure. To create a contour-plot of the iso-damage curves in the P-I plane, a set of calculations has to be carried out. In Fig. 8a, the range of parameters was $0 < I < 15$ kPa·s and $0 < P_{max} < 70$ MPa in increments of ΔI =0.25 kPa·s and $\Delta P_{max} = 1$ MPa. Also shown in Fig. 8 as a dotted line is the pressure level $P = (\sigma_y h)/(2R)$, below which no plastic deformation is possible. This pressure is based on a dynamic load factor of two and a fixed value of yield stress.

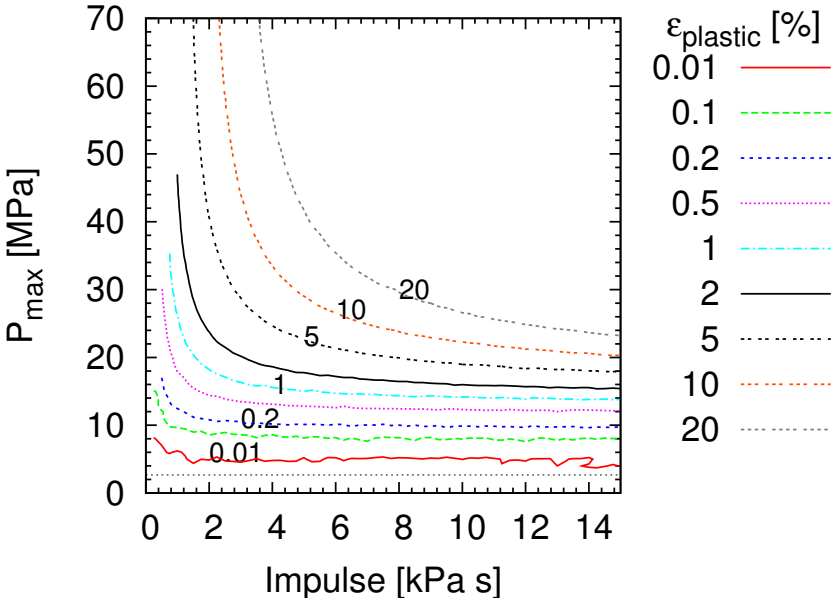

a) CIT "thin tube" geometry. With strain rate effects.

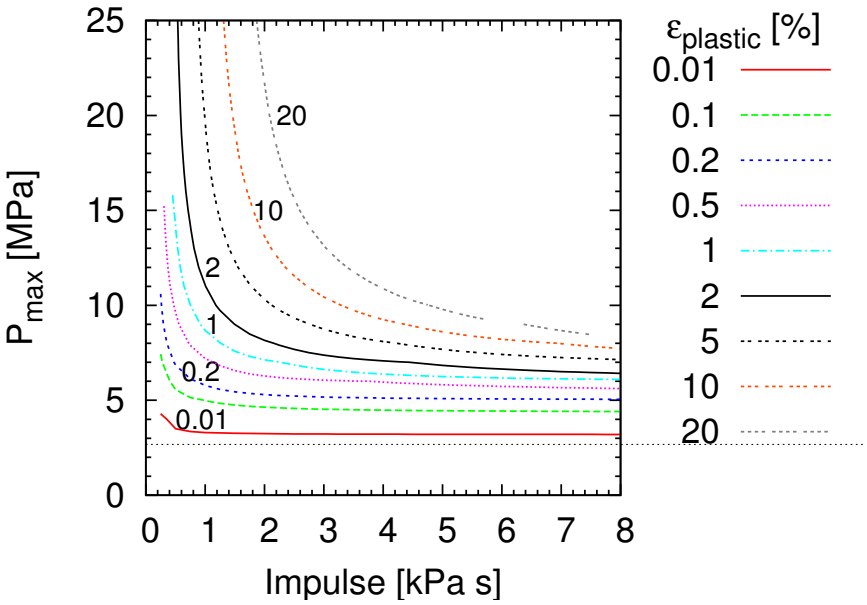

b) CIT "thin tube" geometry. Without strain rate effects.

Figure 8: Pressure impulse diagram showing iso-damage curves for CIT "thin tube" geometry. Note the different scale for (a) and (b). a) With strain rate effects. b) Without strain rate effects.

The iso-damage curves become steeper for lower impulses, which correspond to shorter decay times. This is characteristic of the short pulse or impulse regime and the peak strain is mainly dependent on the impulse and much less dependent on the peak pressure. For larger impulses, and correspondingly larger pulse lengths τ, the iso-damage curves are flatter. This indicates that the resulting strain is more dependent on the peak pressure than the total impulse, characteristic of the long-duration pulse loading regime. The CIT "thin tube" experiments are in the intermediate regime.

Note that the experimental pressure signal does not exactly follow the exponential decay, but the parameters peak pressure P_{max} and decay time τ seem to capture the characteristics which govern the plastic deformation. In order to demonstrate the large influence of the strain rate effects in the material model, Fig. 8b shows the same iso-damage curves assuming no strain rate effects. Note the different scale of the axis in Fig. 8a and b, as the same damage is predicted for much lower impulse and peak pressure when the strain rate effects are neglected. Clearly, strain rate effects are significant for these tests and must be included to obtain realistic values of the final deformation.

5 Two Dimensional Simulations

The simulations presented in the previous section were all one-dimensional, assuming an axially uniform load on the cylindrical shell. In the experiments, the loads due to DDT are observed to be localized and only extend over a finite axial distance. Following the DDT event, a propagating detonation is produced that results in a traveling load. In the present study, we have focused on the loads due to the DDT event. There is extensive discussion for the elastic situation of a traveling load in Beltman et al. (1999), Beltman and Shepherd (2002), Chao and Shepherd (2005a) and we do not consider this further in the present study.[2]

In this section, the results of two-dimensional simulations for static and transient loads of a finite-axial extent are presented. The simulations were carried out with the commercial finite element code LSDYNA. The material properties were taken to be identical to the ones presented in the previous section (Fig. 5). In a DDT event, the load is not uniform over the entire tube length, but is only imparted on a restricted portion of the shell structure. The purpose of the calculations presented in this section are to quantify the influence of the length of the loaded section (w in Fig. 9) on the maximum strain. The 1D case corresponds to infinite load length. As in the previous chapter, rotational symmetry of the load is assumed. A parametric study for various load lengths, peak pressures, and pulse durations is carried out for the CIT "thin tube" and "thick tube" geometries for the elastic and plastic regimes. A rectangular pulse pressure-time history with peak pressure P_{max} and pulse duration τ is assumed. The parameters examined were load lengths w/D =10, 2.5, 1.2, 0.6, 0.3 and 0.15; pulse durations τ =1, 5, 10, 50, 100 and 1000 μs; and pressures P_{max} = 3, 10 and 30 MPa. The impulse for the exponentially decaying pulse is just $I = P_{max}\tau$.

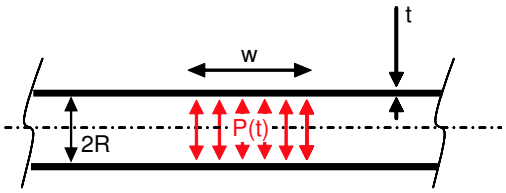

Figure 9: Long cylindrical tube loaded over a length w with circumferentially symmetric pressure $P(t)$.

5.1 Static solution

As a first step, the static solution to a long, thin-walled cylindrical shell under axi-symmetric radial load P over length w was calculated, Fig. 9. An analytical elastic solution to this

[2]Note that the previous studies were all carried in the elastic regime and the situation of a traveling load in the plastic regime is the subject of ongoing study.

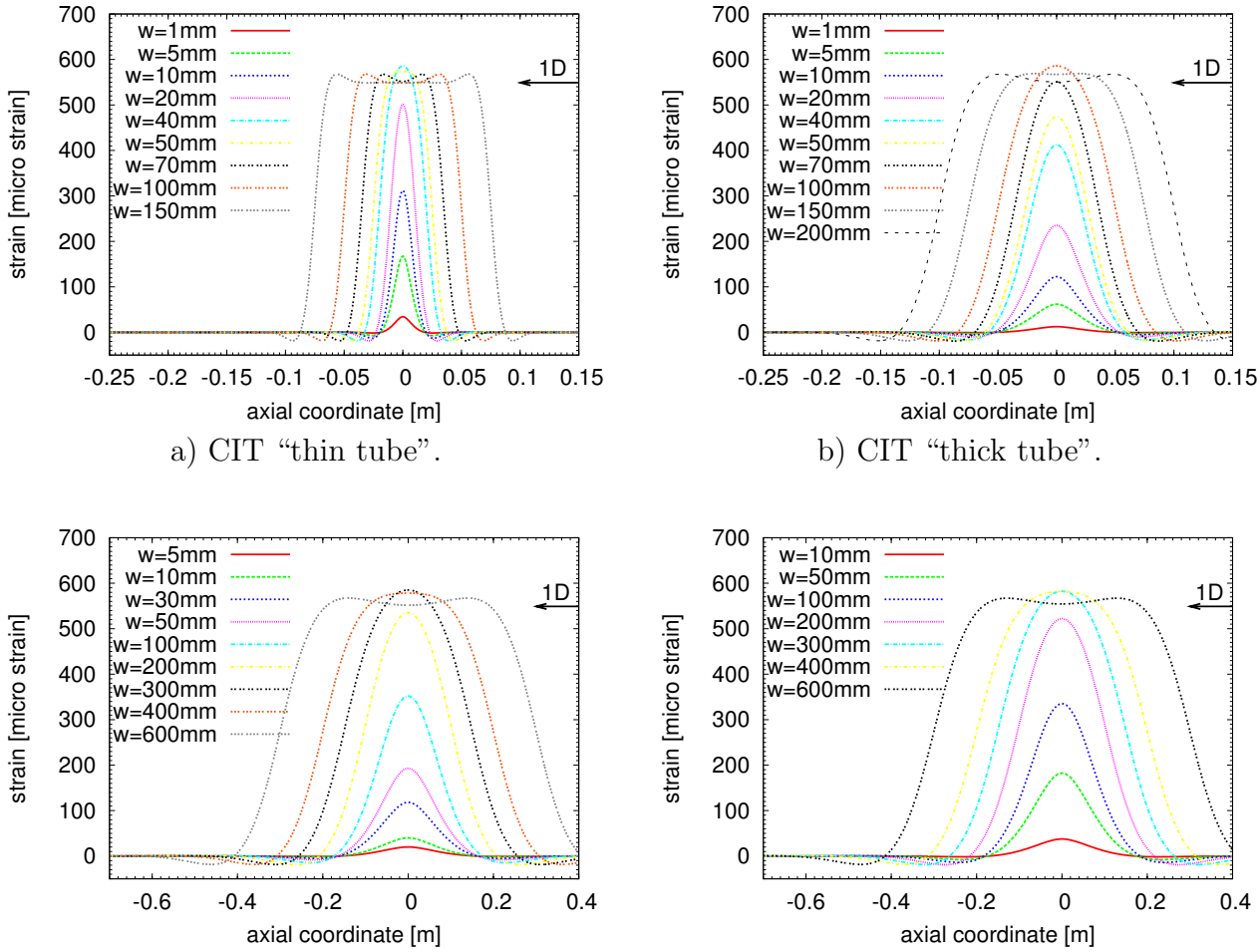

a) CIT "thin tube". b) CIT "thick tube".

c) ARA facility. d) Full scale reactor.

Figure 10: Analytic elastic solution to thin cylindrical shell with a finite length internal load. The peak pressure is chosen to result in the same strain $\epsilon = 500\mu$ for infinite load length in all cases. a) CIT "thin tube" geometry, $P = 3$ MPa. b) CIT "thick tube", $P = 23$ MPa. c) ARA facility geometry, $P = 38$ MPa. d) Full scale reactor geometry, $P = 8$ MPa.

problem is given by Young and Budynas (2002). The resulting hoop strain for various load lengths for all four tube geometries under consideration is shown in Fig. 10. The pressures for the different tube geometries shown in Fig. 10a-d are chosen to result in the same strain of $\epsilon = 550\ \mu$ for infinite load length w. This strain corresponds to the 1D static result of $\epsilon_{1D\ \text{static}}$ given in Appendix 3. For a sufficiently large load length, the deflection is close to the one dimensional result. The peak deflection decreases with decreasing load length once the load length is less than a critical value. For all cases, the highest strain is observed close to the center of the loaded region. Plotting the maximum strain, normalized by the one dimensional solution, as a function of the load length w shows qualitatively similar behavior of all geometries, Fig. 11a. We refer to the normalized strain as a "Load Length Factor"

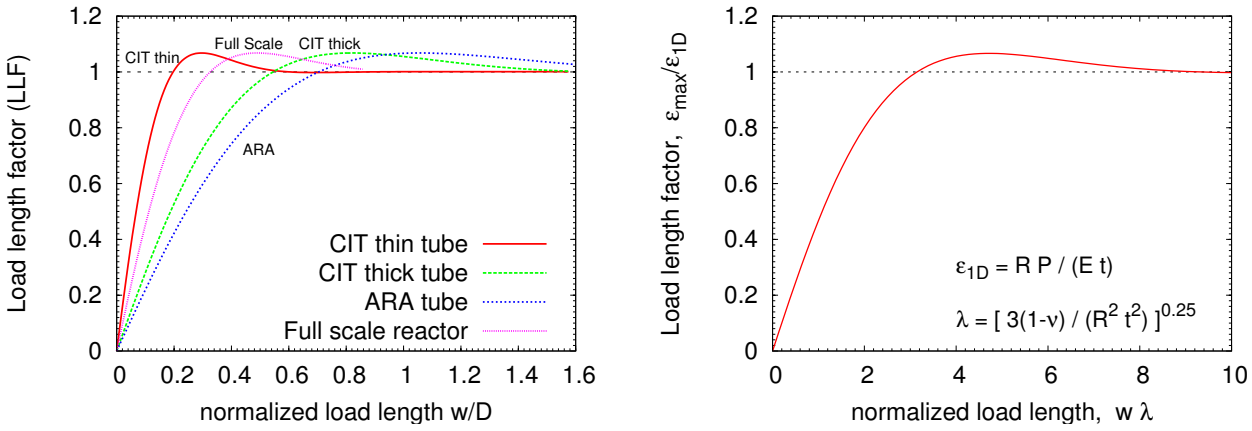

Figure 11: a) Normalized maximum strain, Load length factor (LLF), for all tube geometries as a function of normalized load length w/D. b) Load length factor collapsed by scaling the load length with λ.

($LLF = \epsilon_{max}/\epsilon_{1D}$) since describes the influence of the load length w. For large w, $LLF = 1$ and the one dimensional solution is recovered. For decreasing w, the LLF decreases. For the CIT "thin tube" the load length has to be $w < 0.2D$ in order to see an influence of the load length on the resulting maximum elastic strain. The LLF curves of all geometries can be collapsed, Fig. 11b and Appendix B, if the load length is scaled not by the tube diameter but instead (Young and Budynas, 2002) with the parameter λ

$$\lambda = \left(\frac{3(1-\nu^2)}{R^2 h^2} \right)^{1/4} . \tag{114}$$

This parameter is widely used in the analysis of cylindrical shells to determine the effect of end conditions and other localized bending loads. The physical interpretation is that the distance λ^{-1} is the characteristic length over which localized bending loads decay. When $w\lambda > 5$, the peak deflection becomes independent of the length of the load and deformation in the center of the loaded region can be quantitatively predicted using simple one-dimensional models that treat the loading as being infinite in axial extent, i.e., neglecting the bending due to the finite extent of the load.

5.2 Dynamic elastic calculations

The two-dimensional dynamic simulations were carried out for a tube length of $L = 1.24$ m, corresponding to the size of the CIT "thin tube" and "thick tube" used in the experiments. The loaded section is always centered at the half tube length of $x = 0.62$ m. Built-in boundary

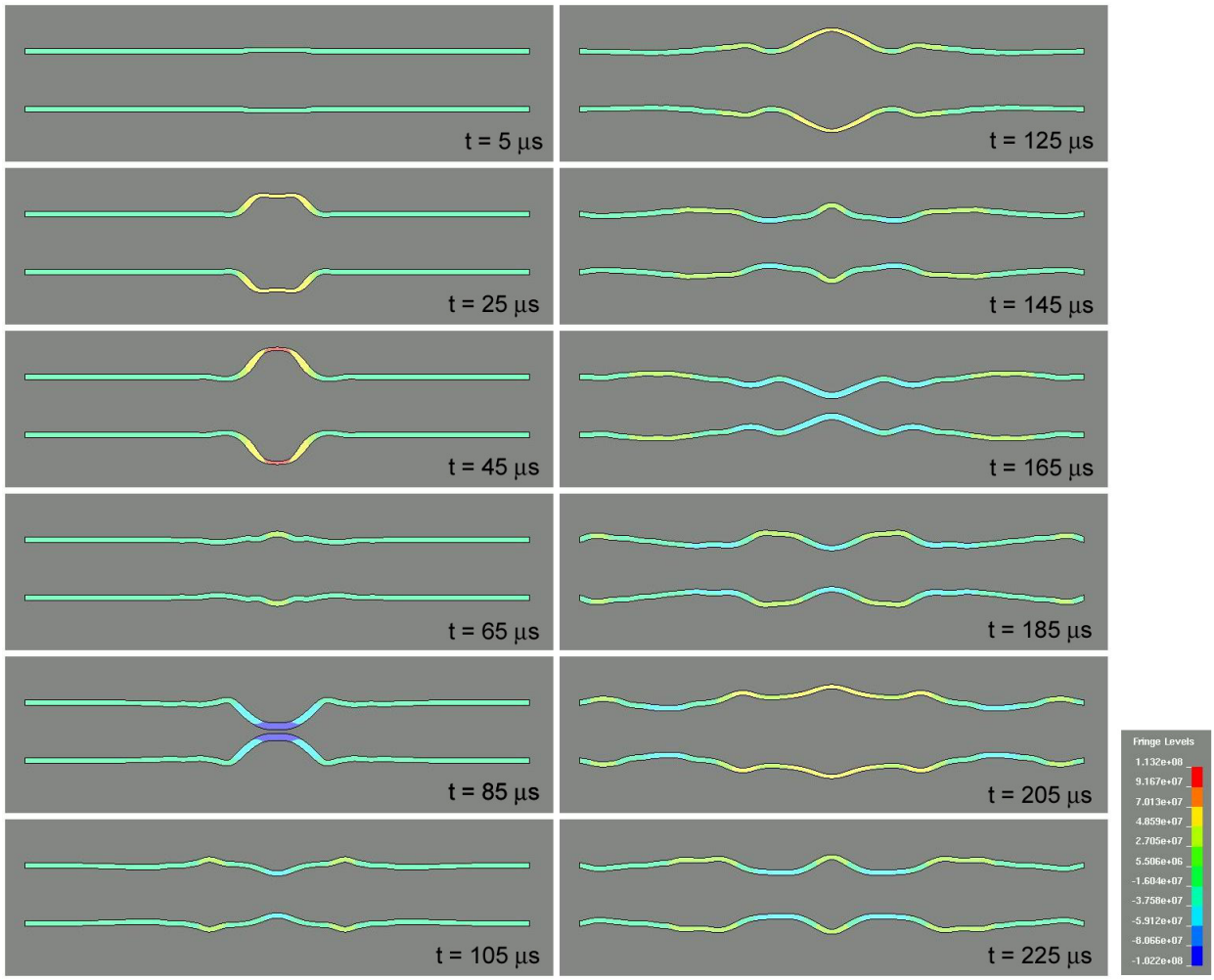

Figure 12: Time sequence of displacements for a two-dimensional finite element simulation of the CIT "thick tube", tube length $L = 1.24$ m, $w = 0$ .155 m, $\tau = 50$ μs, $P_{max} = 10$ MPa (rectangular pulse). The actual displacements are scaled by a factor of 2000 for visibility. The fringe component in the images and scale given on the right correspond to the hoop stress in Pa.

conditions at the tube ends were used for the all calculations, allowing no translational movement for the nodes at the boundary. In the elastic regime, peak pressures of $P_{max} = 3$ and 10 MPa were used for the "thin" and "thick tube", respectively. The rapid application and finite duration of the load makes the solution essentially different from the static case. The history of the deformation is shown as a series of snapshots in Fig. 12. Initially the tube section in the centrally loaded region is displaced outward and the deformation superficially (Fig. 12, $t = 25$ μs) resembles the static case. After the load is removed at 50 μs, flexural waves are observed to propagate away from the loaded section, and toward the ends where they reflect. The reflected and incident waves interfere with each other, resulting in a complex

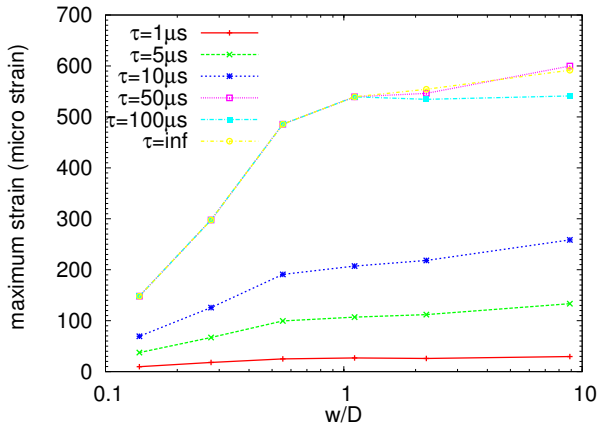

Figure 13: Maximum strain for rectangular pressure pulse of $P_{max} = 10$ MPa applied to the CIT "thick tube" as a function of normalized load length w/D for various pulse durations τ.

displacement pattern. The maximum displacement and strain are observed near the center of the loaded tube section shortly after the pressure pulse is applied. For statically-loaded cylindrical shell structures, the maximum stress is observed on the inner surface of the tube, see Appendix 3. For the CIT "thick tube" geometry, the difference between the stress on the inner and outer surface is 18%, whereas the difference is found to be negligible for the "thin tube".

Plotting (Fig. 13) the maximum strain as a function of w for various pulse durations τ shows that for the "thick tube", the maximum strain is fairly independent of w for $w/D > 0.5$. This is to be expected based on the static load length factor, which is also approximately constant ($LLF \approx 1$) in this regime, Fig. 11a. For a long pulse duration, $\tau \geq 50$ μs, the sudden loading regime with a dynamic load factor of 2 is reached, Fig. 3. The maximum strains for those cases in which $\tau \geq 50$ μs, are nearly identical over the entire range of load lengths examined. Motivated by these two observations, we propose to treat the effects of load length w and pulse duration τ independently. For an estimate of the maximum strain ϵ_{max}, we propose that this can be based on the product of the load-length and dynamic load factors times the one-dimensional static deformation,

$$\epsilon_{max} = \epsilon_{\text{1D static}} \;\; LLF(w) \;\; DLF(\tau). \tag{115}$$

The peak strain estimate based on Eq. 115 is in good agreement with the two dimensional finite element simulations, Fig. 14. We conclude that in the elastic regime, the effects of load length and pulse duration can be treated independently.

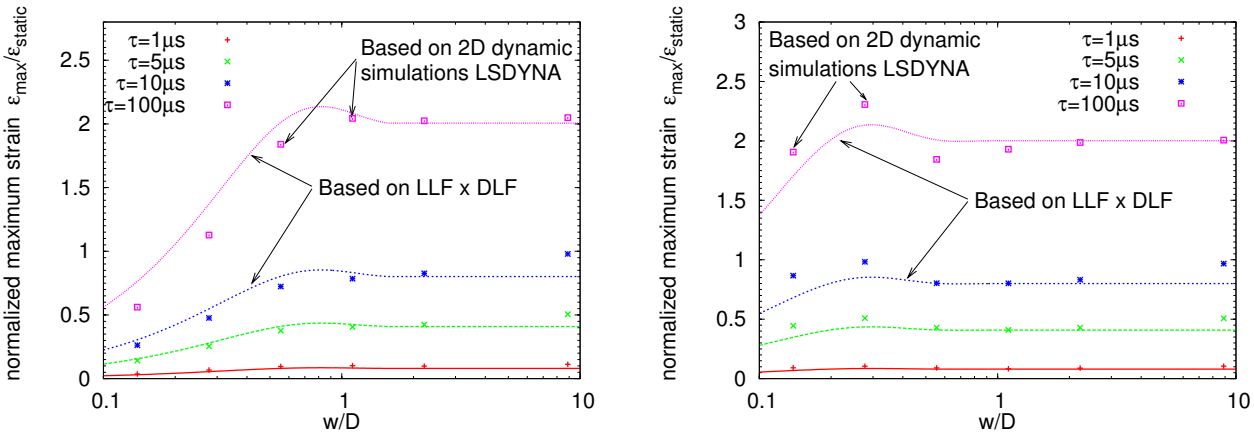

Figure 14: Maximum strain for rectangular pressure pulse of a) $P_{max} = 10$ MPa applied to the CIT "thick tube" and b) $P_{max} = 3$ MPa applied to the CIT "thin tube" as a function of normalized load length w/D for various pulse durations τ compared to the estimate based on Eq. 115.

5.3 Dynamic plastic calculations

The computations of the previous section were repeated using high pressures and the strain-hardening model of an elastic-plastic solid used in previous sections; no strain rate effects were included.

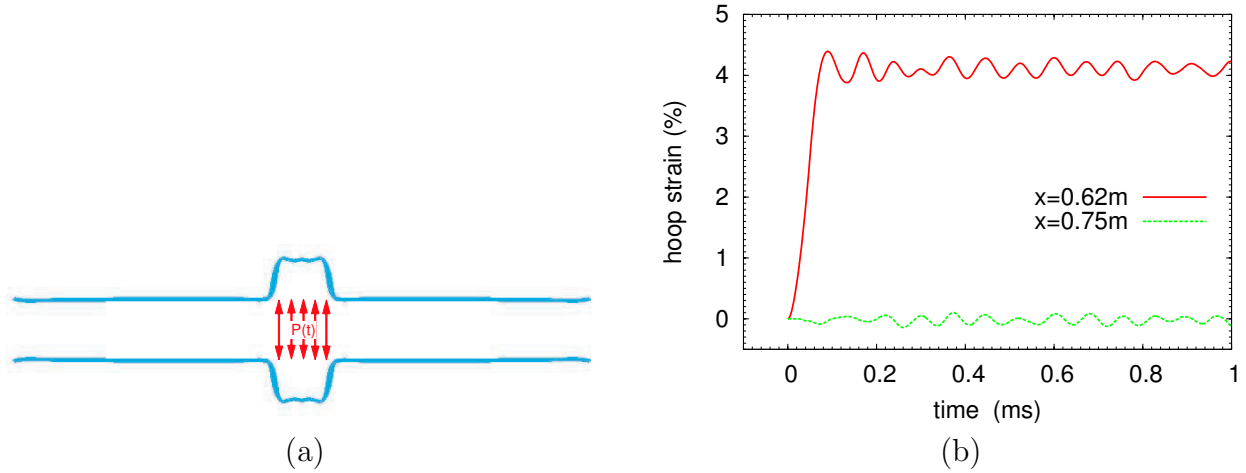

Figure 15: a) Final plastic deformation of "thin tube", $P_{max} = 30$ MPa, $\tau = 50$ ms, $w = 0.15$ m. Displacements scaled by a factor of 30, wall thickness not to scale. b) Hoop strain history in center of loaded region 0.54 m $< x <$ 0.69 m and outside the loaded region at $x = 0.75$ m, $P_{max} = 30$ MPa, $\tau = 50$ ms, $w = 0.15$ m.

In order to create plastic deformation in the simulations using the "thin tube" geometry, the peak pressure of the rectangular pulses was increased to $P_{max} = 30$ MPa, ten times larger

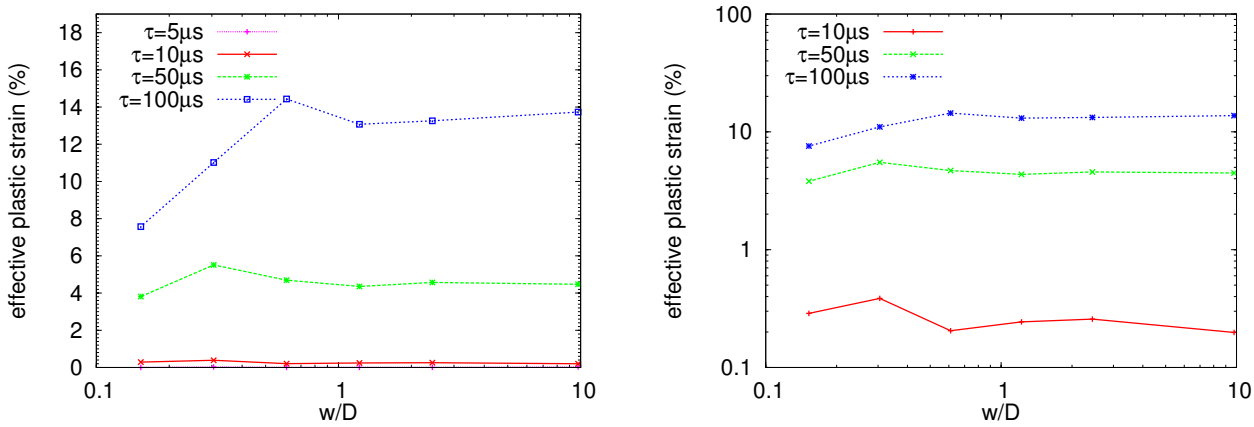

Figure 16: Maximum plastic deformation as a function of w/D for the CIT "thin tube", $P_{max} = 30$ MPa. a) Linear scale b) Logarithmic scale.

than the peak of 3 MPa used in the elastic regime. The plastic deformation is observed to take place only in the immediate vicinity of the loaded section, Fig. 15a. Outside the loaded section, only elastic flexural waves are observed, Fig. 15b. Plotting the maximum plastic strain as a function of load length shows that for $\tau = 100$ μs, the maximum strain decreases by 50% for a load length of $w/D = 0.15$ compared to infinite load length, Fig. 16a. This is a substantial reduction compared to the elastic load length factor $LLF \approx 1$ for $w/D >> 0.15$. Based on this limited comparison, the plastic deformation seems to more affected by the load length than in the corresponding elastic case. The decrease in deformation with decreasing load length is more pronounced for larger pulse durations and correspondingly larger deformations. For $\tau \leq 50$ μs, the plastic deformation is fairly independent of w. We have not attempted to extend the proposed elastic approximation (Eq. 115) to correlate deformation in the plastic regime.

Bibliography

F. Auslender and A. Combescure. Spherical elastic-plastic structures under internal explosion. approximate analytical solutions and applications. *Engineering Structures*, 22: 984–992, 2000.

W. E. Baker, P. A. Cox, P. S. Westine, J. J. Kulesz, and R. A. Strehlow. *Explosion Hazards and Evaluation*. Elsevier, 1983.

W.M. Beltman and J.E. Shepherd. Linear elastic response of tubes to internal detonation loading. *Journal of Sound and Vibration*, 252(4):617–655, 2002.

W.M. Beltman, E. Burcsu, J.E. Shepherd, and L. Zuhal. The structural response of cylindrical shells to internal shock loading. *Journal of Pressure Vessel Technology*, pages 315–322, 1999.

R. A. Benham and T.A. Duffey. Experimental-theoretical correlation on the containment of explosions in cylindrical vessels. *Int. J. Mech. Sci.*, 16:549–558, 1974.

J. Biggs. *Introduction to structural dynamics*. McGraw-Hill, Inc., 1964. ISBN 07-005255-7.

R. D. Blevins. *Formulas for natural frequency and mode shape*. van Nostrand Reinhold Company, 1979.

T. Chao and J.E. Shepherd. Detonation loading of tubes in the modified shear wave regime. In Z. Jiang, editor, *Proceedings of the 24th International Symposium on Shock Waves*, volume 2, pages 865–870. Springer, 2005a.

T.-W. Chao and J. E. Shepherd. Fracture response of externally flawed aluminum cylindrical shells under internal gaseous detonation loading. *International Journal of Fracture*, 134 (1):59–90, July 2005b.

G.R. Cowper and P.S. Symonds. Strain hardening and strain rate effcts in the impact loading of cantilever beams. Technical Report 28, Brown University, Division of Applied Mechanics, 1957.

T.A. Duffey. Approximate solutions of an impulsively loaded long cylinder governed by an elastic-plastic material law. *Acta Mechanica.*, 11:45–57, 1971.

T.A. Duffey and R. Krieg. Effects of strain hardening and strain rate sensitivity on the transient response of elastic-plastic rings and cylinders. *Int. J. Mech. Sci.*, 11:825–844, 1969.

T.A. Duffey and D. Mitchell. Containment of explosions in cylindrical shells. *Int. J. Mech. Sci.*, 15:237–249, 1973.

T.A. Duffey, E.A. Rodriguez, and C. Romero. Design of pressure vessels for high-strain rate loading: dynamic pressure and failure criteria. Bulletin 477, Welding Research Council, P.O. Box 1942, New York, NY, 2002.

F. Fanous and L. Greiman. Simplified analysis for impulsively loaded shells. *Journal of Structural Engineering*, 114:885–899, April 1988.

J. R. Florek and H. Benaroya. Pulse-pressure loading effects on aviation and general engineering structures. *Journal of Sound and Vibration*, 284:421–453, 2005.

E. J. Hampton and J. L. Bitner. Stress or strain criteria for combined static and dynamic loading. Bulletin 500, Welding Research Council, P.O. Box 1942, New York, NY, 2005.

J. F. Harvey. *Theory and Design of Modern Pressure Vessels*. Van Nostrand Reinhold Company, second edition, 1974.

P. G. Hodge. The influence of blast characteristics on final deformation of circular cylindrical shells. *Journal of Applied Mechanics*, 284:617–624, December 1956.

W. Johnson and P. B. Mellor. *Engineering Plasticity*. Ellis Horwood Limited, 1983.

N. Jones. *Structural Impact*. Cambridge University Press, 1989. ISBN 0-521-30180-7.

C. Moosbrugger. *Atlas of stress-strain curves*. Materials Park, OH : ASM international, 2002.

W. K. Nowacki. *Stress waves in non-elastic solids*. Oxford. New York, Pergammon Press., 1978.

W.S. Pellini. Design options for selection of fracture control procedures in the modernization of codes, rules and standards. analytical design procedures for metals of elastic-plastic and plastic fracture properties. Bulletin 186, Welding Research Council, P.O. Box 1942, New York, NY, 1973.

E.A. Rodriguez and T.A. Duffey. Fracture-safe and fatigue design criteria for detonation-induced pressure loading in containment vessels. Bulletin 494, Welding Research Council, P.O. Box 1942, New York, NY, 2004.

J. E. Shepherd. Pressure loads and structural response of the BNL high-temperature detonation tube. Technical Report A-3991, Brookhaven National Laboratory, January 1992. 72 pp.

W. Soedel. *Vibrations of Plates and Shells*. Marcel Dekker, Inc., NY, third, expanded and revised edition, 2004.

S.P. Timoshenko and J. N. Goodier. *Theory of Elasticity*. McGraw-HIll Publishing Company, third edition, 1970.

A.C. Ugural and S.K. Fenster. *Advanced Strength and Applied Elasticity*. Elsevier, 2nd si edition, 1987.

W. Young and R. Budynas. *Roark's formulas for stress and strain*. McGraw-Hill, 2002. ISBN 0-07-072542-X. Seventh Edition.

A Dynamic Load Factor

The dynamic load factor for a rectangular pulse on an elastic single-degree-of-freedom system is derived by (Biggs, 1964, p. 42). We reproduce the results here for completeness. The load is applied for a duration τ and the resonant frequency of the system is $\omega = 2\pi/T$.

The normalized deflection X/X_s where X_s is the static response to the same load, is given by

$$X/X_s = 1 - \cos\omega t \tag{116}$$

$$= 1 - \cos 2\pi \frac{t}{T} \tag{117}$$

for $t \leq \tau$ and by

$$X/X_s = \cos\omega(t-\tau) - \cos\omega t \tag{118}$$

$$= \cos 2\pi(\frac{t}{T} - \frac{\tau}{T}) - \cos 2\pi \frac{t}{T} \tag{119}$$

for $t \geq \tau$. The maximum deflection can be determined from these expressions by numerically solving for the time of maximum deflection.

$$\frac{dX}{dt}(t_{max}) = 0 \tag{120}$$

which results in the simple implict equation for t_{max}

$$\sin(\omega t_{max} - \omega\tau) = sin\omega t_{max} \tag{121}$$

$$X_{max} = X(t_{max})\ . \tag{122}$$

The functional dependence of the solution on the combination of $\omega\tau$ clearly shows that both X_{max} and t_{max} are functions of only $\omega\tau$ or equivalently τ/T. Evaluating the scaled deflection at t_{max} yields the dynamic load factor

$$DLF = X_{max}/X_s \tag{123}$$

The results for the DLF as a function of scaled load duration are given in Fig. 3 and Table 2 below. Note that for $\tau > 0.5T$, the $DLF = 2$ independent of the load duration. In other words, as long as the pulse length is greater than one-half of the period of oscillation, the peak deflection is the same as if the pulse length were infinite.

Table 2: Dynamic Load factor for rectangular pulse on a SDOF structure.

τ/T	DLF
0.0502	0.3062
0.0596	0.3614
0.0694	0.4287
0.0791	0.4801
0.0890	0.5434
0.0987	0.6028
0.1191	0.7257
0.1416	0.8645
0.1650	0.9913
0.1844	1.1024
0.2004	1.1897
0.2288	1.3286
0.2611	1.4754
0.3043	1.6421
0.3473	1.7730
0.3963	1.9039
0.4843	1.9949
0.5832	2.0000
0.6926	2.0000
0.8873	2.0000
0.9838	2.0000
1.4868	2.0000
2.9589	2.0000
9.9327	2.0000

B Load-Length Factor

The load length factor for a finite length axi-symmetric load can be computed using the elastic solution presented in Young and Budynas (2002). The parameters that enter into this computation are

Y	radial displacement
w	load length
R	tube radius
h	tube thickness
E	Young's modulus
ν	Poisson ratio

The reciprocal of the shell scaling length is

$$\lambda = \left[\frac{3(1-\nu^2)}{R^2h^2}\right]^{1/4} . \tag{124}$$

The shell flexural rigidity is

$$D = \frac{Eh^3}{12(1-\nu^2)} . \tag{125}$$

The deflection of a one-dimensional shell subject to an internal load pressure P is

$$X_{1D} = \frac{R^2P}{Eh} \tag{126}$$

$$= \frac{P}{4D\lambda^4} . \tag{127}$$

The load length factor is defined as

$$LLF = \frac{X}{X_{1D}} \tag{128}$$

The results are given in graphical form in Fig. 11 and in the following table using material parameters corresponding to the mild steel used in the thin-tube experiments.

Table 3: Load length factor as a function of normalized load width.

$w\lambda$	LLF
0	0
0.125539	0.062661399
0.251078	0.124863625
0.376617	0.186200514
0.502156	0.246320223
0.627695	0.304921431
0.753234	0.361749601
0.878773	0.416593348
1.004312	0.469280914
1.129851	0.519676761
1.25539	0.567678301
1.380929	0.613212769
1.506468	0.656234244
1.632007	0.696720819
1.757546	0.734671932
1.883085	0.770105851
2.008624	0.803057319
2.134163	0.83357535
2.259702	0.861721185
2.385241	0.887566397
2.51078	0.911191139
2.636319	0.932682542
2.761858	0.952133245
2.887397	0.969640059
3.012936	0.985302761
3.138475	0.999223003
3.264014	1.01150334
3.389553	1.022246364
3.515092	1.031553941
3.640631	1.03952654
3.766170	1.046262659
3.891709	1.051858325
4.017248	1.056406676
4.142787	1.059997613
4.268326	1.062717514
4.393865	1.064649015
4.519404	1.065870836
4.644943	1.066457662
4.770482	1.066480067
4.896021	1.066004474

$w\lambda$	LLF
5.02156	1.065093157
5.147099	1.063804266
5.272638	1.062191885
5.398177	1.060306113
5.523716	1.058193159
5.649255	1.055895464
5.774794	1.053451827
5.900333	1.050897552
6.025872	1.048264594
6.151411	1.045581722
6.27695	1.04287468
6.402489	1.040166353
6.528028	1.037476936
6.653567	1.034824102
6.779106	1.032223168
6.904645	1.029687258
7.030184	1.027227469
7.155723	1.024853025
7.281262	1.022571428
7.406801	1.02038861
7.53234	1.018309071
7.657879	1.016336017
7.783418	1.014471486
7.908957	1.012716474
8.034496	1.011071048
8.160035	1.009534457
8.285574	1.008105232
8.411113	1.006781282
8.536652	1.005559987
8.662191	1.004438273
8.78773	1.003412694
8.913269	1.002479497
9.038808	1.001634689
9.164347	1.000874094

$w\lambda$	LLF
9.289886	1.000193407
9.415425	0.999588237
9.540964	0.999054153
9.666503	0.998586721
9.792042	0.998181538
9.917581	0.997834257
10.04312	0.997540617
10.168659	0.997296463
10.294198	0.997097764
10.419737	0.996940627
10.545276	0.996821313
10.670815	0.99673624
10.796354	0.996682
10.921893	0.996655357
11.047432	0.996653251
11.172971	0.996672803
11.29851	0.996711313
11.424049	0.99676626
11.549588	0.996835298
11.675127	0.996916253
11.800666	0.997007121
11.926205	0.997106059
12.051744	0.997211383
12.177283	0.99732156
12.302822	0.997435203
12.428361	0.997551061
12.553900	0.997668015
12.679439	0.997785071
12.804978	0.997901351
12.930517	0.998016085
13.056056	0.998128606
13.181595	0.998238344
13.307134	0.998344814
13.432673	0.998447614

$w\lambda$	LLF
13.558212	0.998546416
13.683751	0.99864096
13.80929	0.99873105
13.934829	0.998816543
14.060368	0.99889735
14.185907	0.998973426
14.311446	0.999044765
14.436985	0.999111398
14.562524	0.999173389
14.688063	0.999230824
14.813602	0.999283818
14.939141	0.999332501
15.06468	0.999377022
15.190219	0.999417543
15.315758	0.999454235
15.441297	0.999487279
15.566836	0.999516861
15.692375	0.999543169
15.817914	0.999566397
15.943453	0.999586734
16.068992	0.999604373
16.194531	0.999619499
16.32007	0.999632299
16.445609	0.999642952
16.571148	0.999651631
16.696687	0.999658507
16.822226	0.99966374
16.947765	0.999667486
17.073304	0.999669893
17.198843	0.9996711
17.324382	0.99967124
17.449921	0.999670439
17.57546	0.999668813
17.700999	0.999666471

$w\lambda$	LLF
17.826538	0.999663515
17.952077	0.99966004
18.077616	0.999656133
18.203155	0.999651873
18.328694	0.999647334
18.454233	0.999642581
18.579772	0.999637676
18.705311	0.999632673
18.83085	0.999627621
18.956389	0.999622561
19.081928	0.999617534
19.207467	0.999612572
19.333006	0.999607704
19.458545	0.999602955
19.584084	0.999598347
19.709623	0.999593896
19.835162	0.999589618
19.960701	0.999585523
20.08624	0.99958162
20.211779	0.999577916
20.337318	0.999574414
20.462857	0.999571116
20.588396	0.999568023
20.713935	0.999565134
20.839474	0.999562445
20.965013	0.999559953